Dead Sea Workshop

16th- 23rd February 2009

The Dead Sea Rift as a natural laboratory for earthquake behavior: prehistorical, historical and recent seismicity

Organized by

Rivka Amit, Geological Survey of Israel

Alessandro M. Michetti, INQUA Paleoseismology Subcommission

Co-organizers: Amotz Agnon, Ari Matmon, The Hebrew University of Jerusalem

Edited by:
Rivka Amit
Amotz Agnon
Ari Matmon

In collaboration with:

UNESCO
Geological Survey of Israel
Safed Scientific Workshop Program
Hebrew University of Jerusalem
The Israel Geological Society
Israel National Earthquake Preparedness Committee
University of Missouri, Kansas City USA

Acknowledgment:

The field guide was made possible through the financial support of the Geological Survey of Israel. We thank Yoav Nahamias for his outstanding help in the workshop organization. Thanks to Shalev Siman-Tov for his technical assistance and contribution in preparing the figures, Rani Calvo and Shalev Siman-Tov for providing photographs, Rami Madmon, Yaacov Mizrahi and Yaacov Refael for their technical assistance. We specially thank Avner Ayalon for his editorial assistance, Bat-Sheva Cohen, Chana Netzer-Cohen and Nili Almog for their editorial and graphical design of the field guide.

Contents

Arava valley (pages 127-205)

- The structure of the western margin of the Dead Sea Rift, southern Arava Valley
- Geodetic and geophysical background of the Arava Valley
- Late Quaternary seismicity of the Southern Arava Valley, the Dead Sea Fault
- Landscape development in a hyper arid sandstone environment along the margins of the Dead Sea Fault: implications from dated rock falls
- Reconstructing active rift margin tectonics using cosmogenic exposure age dating of desert pavements: Quaternary subsidence along the western margin of the Dead Sea Rift

Judean Mountains (pages 207-212)

- Speleoseismology in the Soreq Cave: The first dated ultra-long record of strong earthquakes

Introduction - The Dead Sea Fault

Shmuel Marco

The Department of Geophysics and Planetary Sciences, Tel Aviv University.

E-mail: shmulikm@tau.ac.il

The Dead Sea Fault (DSF) accommodates sinistral motion between the Arabia plate and the Sinai subplate since the Middle Miocene, ~20 Ma. The interpretation of 107 km left-lateral slip along the DSF is based on observations from four independent sources: regional plate tectonics, local geology, seismology, and geodesy. The regional tectonics shows that the Red Sea is an incipient ocean, where the Arabian plate has been breaking away from Africa since Late Oligocene-Early Miocene. This motion is transferred to the collision with Eurasia via sinistral shear along the DSF (Courtillot et al., 1987; Freund, 1965; Garfunkel, 1981; Joffe and Garfunkel, 1987; Quennell, 1956). Local geology shows systematic offset of numerous pre-Miocene geologic features by a total of ~107 km (Bartov et al., 1980; Freund, 1965; Quennell, 1956) and fault geometry that indicates left-lateral motion (Garfunkel, 1981). Paleoseismic and archaeoseismic studies show sub-recent activity as sinistral offsets of natural and of manmade structures (e.g., Amit et al., 2002; Ellenblum et al., 1998; Klinger et al., 2000; Meghraoui et al., 2003; Niemi et al., 2001). Focal mechanisms of moderate-to-large earthquakes show sinistral motion along the DSF and generally are in agreement with the location of the active faults, based on geological data (Baer et al., 1999; Hofstetter et al., 2007; Klinger et al., 1999; Salamon et al., 1996). And finally, geodetic measurements are consistent and confirm the left-lateral slip as well as the slip rate from other palaeoseismic evidence of 4±1 mm/yr (Le Beon et al., 2006; Le Beon et al., 2008; McClusky et al., 2003; Reilinger et al., 2006; Wdowinski et al., 2004). This rate, as well as uniform Gutenberg-Richter frequency-magnitude relation, indicate stable tectonic regime in the last 60 ka (Begin et al., 2005; Hamiel et al., 2008).

The complex geometry of the fault is apparent in pull-apart grabens, which are associated with releasing bends, and pressure ridges that formed where restraining bends occur. Garfunkel (1981) maintains that the pull-apart basins are all shorter the total lateral offset because they began to

form at a later stage, after some motion had already accrued. This view is supported by seismic surveys that reveal earlier buried basins, which are no longer active (Frieslander, 2000).

The pull-apart basins have acted like sediment traps. Studies of the Miocene to Recent clastic and evaporitic sediments as well as some magmatic sequences that accumulated in the basins have yielded a wealth of information and insight on the history of sedimentological conditions and processes (e.g., Bookman et al., 2004; Frostick and Reid, 1989; Klinger et al., 2003; Sneh, 1981, 1982; Tsatskin and Nadel, 2003), climate (e.g., Bartov et al., 2003; Begin et al., 1974; Frumkin et al., 1991; Stein, 2001), geomagnetic secular variation (Marco et al., 1998), seismicity and deformation (e.g., Agnon et al., 2006; Bartov and Sagy, 2004; El-Isa and Mustafa, 1986; Heifetz et al., 2005; Ken-Tor et al., 2001; Marco et al., 1996; Migowski et al., 2004), fauna and flora (Kislev et al., 1992), humans, and environment (e.g., Braun et al., 1991; Goren-Inbar and Belitzky, 1989; Goren-Inbar et al., 2000; Ron and Levi, 2001).

Several authors noted that the detailed shape of the DSF had changed through time (Garfunkel, 1981; Heimann and Ron, 1987, 1993; Marco, 2007; Rotstein et al., 1992; Shamir et al., 2005; ten Brink et al., 1999; ten-Brink and Ben-Avraham, 1989). The widest zone of about 50 km of distributed faulting is found in the Galilee, where the early-stage (Miocene) faults were associated with formation of basins (Freund et al., 1970; Shaliv, 1991) and with rotation of rigid blocks about sub-vertical axes (Ron et al., 1984). Subsequent post-Miocene deformation took place mostly in the form of normal faulting on E-W trending faults and the transform movement is currently localized in a very narrow zone. The deformation in the south was characterized initially by a 20-30-km-wide zone with primarily strike-slip and some normal slip on faults trending sub-parallel to the main transform fault. It later became localized in the Arava, where a single narrow fault zone offsets the youngest alluvium. In the earliest phase, young faults became active in the Negev, some 20 km west of the Arava (Avni et al., 2000), perhaps indicating another widening phase of the DSF zone (Marco, 2007).

Table 1. Various estimates of the Dead Sea Fault slip rate

Period	Rate mm/y	Data	Reference
Late Pleistocene-Recent	10	Geological	(Freund et al., 1968)
Last 1000 yr	0.8-1.7	Historical	(Garfunkel et al., 1981)

Plio-Pleistocene	7-10	Geological	(Garfunkel et al., 1981)
Last 4500 yr	2.2	Seismicity	(Ben-Menahem, 1981)
Late Pleistocene	6.4±0.4	Seismicity	(El-Isa and Mustafa, 1986)
Plio-Pleistocene	6 (0.283°/ma)	Plate kinematics	(Joffe and Garfunkel, 1987)
Holocene	9	Geological	(Reches and Hoexter, 1981)
Plio-Pleistocene	20	Geological	(Steinitz and Bartov, 1986)
Holocene	>0.7	Geological	(Gardosh et al., 1990)
Plio-Pleistocene	5.4-6.1	Geological	(Heimann, 1990)
Plio-Pleistocene	3-7	Drainage systems, Arava Fault	(Ginat et al., 1998)
Pleistocene	2-6, prefer 4	Alluvial fans, N. Arava	(Klinger et al., 2000)
Pleistocene	4.7±1.3	Alluvial fans, Arava	(Niemi et al., 2001)
Last 2000 yrs	6.9±0.1	Paleo and Archaeoseismology, Missyaf (DSF in Syria)	(Meghraoui et al., 2003)
1996-1999	2.6±1	Geodesy, GPS	(Pe'eri et al., 2002)
1996-2003	3.3±0.4	Geodesy, GPS	(Wdowinski et al., 2004)
25 ka	3.8–6.4	Geological, Lebanon	(Daëron et al., 2004)
Last 5000 yrs	≥3	Stream channel, Jordan Gorge	(Marco et al., 2005)
Survey-Mode GPS	5.6 to 7.5	(from south to north)	(McClusky et al., 2003)
1999-2005	4.9±1.4	GPS	(Le Beon et al., 2008) and thesis
Last 47.5 kyrs	4.7 to 5.1 mm/yr	Offset channels, Jordan	(Ferry et al., 2007) Comment/Reply: (Ferry and Meghraoui, 2008; Klein, 2008)

References

Agnon, A., Migowski, C., and Marco, S., 2006, Intraclast breccia layers in laminated sequences: recorders of paleo-earthquakes, *in* Enzel, Y., Agnon, A., and Stein, M., eds., New Frontiers in Dead Sea Paleoenvironmental Research, Geological Society of America Special Publication, p. 195-214.

Amit, R., Zilberman, E., Enzel, Y., and Porat, N., 2002, Paleoseismic evidence for time dependency of seismic response on a fault system in the southern Arava valley, Dead Sea rift, Israel: Geol. Soc. Am. Bull., v. 114, p. 192-206.

Avni, Y., Bartov, Y., Garfunkel, Z., and Ginat, H., 2000, Evolution of the Paran drainage basin and its relation to the Plio-Pleistocene history of the Arava Rift western margin, Israel: Isr. J. Earth Sci., v. 49, p. 215-238.

Baer, G., Sandwell, D., Williams, S., Bock, Y., and Shamir, G., 1999, Coseismic deformation associated with the November 1995, Mw = 7.1 Nuweiba earthquake, Gulf of Elat (Aqaba), detected by synthetic aperture radar interferometry: J. Geophys. Res., v. 104, p. 25,221-25,232.

Bartov, Y., Goldstein, S.L., Stein, M., and Enzel, Y., 2003, Catastrophic arid episodes in the Eastern Mediterranean linked with the North Atlantic Heinrich events: Geology, v. 31, p. 439-442.

Bartov, Y., and Sagy, a., 2004, Late Pleistocene extension and strike-slip in the Dead Sea Basin: Geological Magazine, v. 141, p. 565-572.

Bartov, Y., Steinitz, G., Eyal, M., and Eyal, Y., 1980, Sinistral movement along the Gulf of Aqaba - its age and relation to the opening of the Red Sea: Nature, v. 285, p. 220-221.

Begin, B.Z., Steinberg, D.M., Ichinose, G.A., and Marco, S., 2005, A 40,000 years unchanging of the seismic regime in the Dead Sea rift: Geology, v. 33, p. 257-260.

Begin, Z.B., Ehrlich, A., and Nathan, Y., 1974, Lake Lisan, the Pleistocene precursor of the Dead Sea: Geol. Surv. Isr. Bull., v. 63, p. 30.

Ben-Menahem, A., 1981, Variation of slip and creep along the Levant Rift over the past 4500 years: Tectonophysics, v. 80, p. 183-197.

Bookman, R., Enzel, Y., Agnon, A., and Stein, M., 2004, Late Holocene lake levels of the Dead Sea: Bull. Geol. Soc. Am., v. 116, p. 555-571.

Braun, D., Ron, H., and Marco, S., 1991, Magnetostratigraphy of the hominid tool bearing Erk el Ahmar formation in the northern Dead Sea Rift: Isr. J. Earth Sci., v. 40, p. 191-197.

Courtillot, V., Armijo, R., and Tapponnier, P., 1987, The Sinai Triple Junction Revisited: Tectonophysics, v. 141, p. 181-190.

Daëron, M., Benedetti, L., Tapponnier, P., Sursock, A., and Finkel, R.C., 2004, Constraints on the post 25-ka slip rate of the Yammouneh fault (Lebanon) using in situ cosmogenic 36Cl dating of offset limestone-clast fans: Earth Planet. Sci. Lett., v. 227, p. 105-119.

El-Isa, Z.H., and Mustafa, H., 1986, Earthquake deformations in the Lisan deposits and seismotectonic implications: Geophys. J. R. Astron. Soc., v. 86, p. 413-424.

Ellenblum, R., Marco, S., Agnon, A., Rockwell, T., and Boas, A., 1998, Crusader castle torn apart by earthquake at dawn, 20 May 1202: Geology, v. 26, p. 303-306.

Ferry, M., and Meghraoui, M., 2008, Reply to the comment of Dr M. Klein on: "A 48-kyr-long slip rate history for the Jordan Valley segment of the Dead Sea Fault": Earth and Planetary Science Letters, v. 268, p. 241-242.

Ferry, M., Meghraoui, M., Abou Karaki, N., Al-Taj, M., Amoush, H., Al-Dhaisat, S., and Barjous, M., 2007, A 48-kyr-long slip rate history for the Jordan Valley segment of the Dead Sea Fault: Earth and Planetary Science Letters, v. 260, p. 394-406.

Freund, R., 1965, A model of the structural development of Israel and adjacent areas since Upper Cretaceous times: Geol. Mag., v. 102, p. 189-205.

Freund, R., Garfunkel, Z., Zak, I., Goldberg, M., Weissbrod, T., and Derin, B., 1970, The shear along the Dead Sea rift: Phil. Trans. Roy. Soc. Lond., v. A. 267, p. 107-130.

Freund, R., Zak, I., and Garfunkel, Z., 1968, Age and rate of the sinistral movement along the Dead Sea Rift: Nature, v. 220, p. 253-255.

Frieslander, U., 2000, The structure of the Dead Sea Transform emphasizing the Arava using new geophysical data [Ph.D. (in Hebrew, English abstract) thesis], The Hebrew University of Jerusalem.

Frostick, L.E., and Reid, I., 1989, Climatic versus tectonic controls of fan sequences: lessons from the Dead Sea, Israel: Jour. Geol. Soc. London, v. 146, p. 527-538.

Frumkin, A., Magaritz, M., Carmi, I., and Zak, I., 1991, The Holocene climatic record of the salt caves of Mount Sedom, Israel: The Holocene, v. 3, p. 191-200.

Gardosh, M., Reches, Z., and Garfunkel, Z., 1990, Holocene tectonic deformation along the western margins of the Dead Sea: Tectonophysics, v. 180, p. 123-137.

Garfunkel, Z., 1981, Internal structure of the Dead Sea leaky transform (rift) in relation to plate kinematics: Tectonophysics, v. 80, p. 81-108.

Garfunkel, Z., Zak, I., and Freund, R., 1981, Active faulting in the Dead Sea rift: Tectonophysics, v. 80, p. 1-26.

Ginat, H., Enzel, Y., and Avni, Y., 1998, Translocation of Plio-Pleistocene drainage system along the Dead Sea Transform, south Israel: Tectonophysics, v. 284, p. 151-160.

Goren-Inbar, N., and Belitzky, S., 1989, Structural position of the Pleistocene Gesher Benot Ya'akov site in the Dead Sea Rift zone: Quaternary Research, v. 31, p. 371-376.

Goren-Inbar, N., Craig, F.S., Verosub, K.L., Melamed, Y., Kislev, M., Tchernov, E., and Saragusti, I., 2000, Pleistocene milestones on the Out-of-Africa Corridor at Gesher Benot Ya'aqov, Israel: Science, v. 289, p. 944-947.

Hamiel, Y., Amit, R., Begin, Z.B., Marco, S., Katz, O., Salamon, A., Zilberman, E., and Porat, N., 2008, The seismicity along the Dead Sea fault during the last 60,000 years: Seismological Society of America Bulletin, v. in press.

Heifetz, E., Agnon, A., and Marco, S., 2005, Soft sediment deformation by Kelvin Helmholtz Instability: A case from Dead Sea earthquakes: Earth Planet. Sci. Lett., v. 236, p. 497-504.

Heimann, A., 1990, The development of the Dead Sea rift and its margins in the northern Israel during the Pliocene and the Pleistocene, Golan Res. Inst. and Geol. Surv. Isr.

Heimann, A., and Ron, H., 1987, Young faults in the Hula pull-apart basin, central Dead Sea transform: Tectonophysics, v. 141, p. 117-124.

—, 1993, Geometric changes of plate boundaries along part of the northern Dead Sea Transform: Geochronologic and paleomagnetic evidence: Tectonics, v. 12, p. 477-491.

Hofstetter, R., Klinger, Y., Amrat, A.Q., Rivera, L., and Dorbath, L., 2007, Stress tensor and focal mechanisms along the Dead Sea fault and related structural elements based on seismological data: Tectonophysics, v. 429, p. 165-181.

Joffe, S., and Garfunkel, Z., 1987, Plate kinematics of the circum Red Sea- a re-evaluation: Tectonophysics, v. 141, p. 5-22.

Ken-Tor, R., Agnon, A., Enzel, Y., Marco, S., Negendank, J.F.W., and Stein, M., 2001, High-resolution geological record of historic earthquakes in the Dead Sea basin: J. Geophys. Res., v. 106, p. 2221-2234.

Kislev, M.E., Nadel, D., and Carmi, I., 1992, Epipalaeolithic (19,000 Bp) Cereal and Fruit Diet at Ohalo-Ii, Sea of Galilee, Israel: Review of Palaeobotany and Palynology, v. 73, p. 161-166.

Klein, M., 2008, A comment on: "A 48-kyr-long slip rate history for the Jordan Valley segment of the Dead Sea Fault" EPSL 260 (2007) 394-406: Earth and Planetary Science Letters, v. 268, p. 239-240.

Klinger, Y., Avouac, J.P., Abou-Karaki, N., Dorbath, L., Bourles, D., and Reyss, J.L., 2000, Slip rate on the Dead Sea transform fault in northern Araba Valley (Jordan): Geophys. J. Int., v. 142, p. 755-768.

Klinger, Y., Avouac, J.P., Bourles, D., and Tisnerat, N., 2003, Alluvial deposition and lake-level fluctuations forced by Late Quaternary climate change: the Dead Sea case example: Sedimentary Geology, v. 162, p. 119-139.

Klinger, Y., Rivera, L., Haessler, H., and Maurin, J.C., 1999, Active faulting in the Gulf of Aqaba: New knowledge from the Mw7.3 earthquake of 22 November 1995: Bull. Seism. Soc. Am., v. 89, p. 1025-1036.

Le Beon, M., Klinger, Y., Agnon, A., Dorbath, L., Baer, G., Meriaux, A.-S., Ruegg, J.-C., Charade, O., Finkel, R., and Ryerson, F., 2006, Geodetic versus geologic slip rate along the Dead Sea, Seismological Society of America Annual Meeting: San Francisco.

Le Beon, M., Klinger, Y., Amrat, A.Q., Agnon, A., Dorbath, L., Baer, G., Ruegg, J.C., Charade, O., and Mayyas, O., 2008, Slip rate and locking depth from GPS profiles across the southern Dead Sea Transform: Journal of Geophysical Research-Solid Earth, v. 113, p. -.

Marco, S., 2007, Temporal variation in the geometry of a strike-slip fault zone: Examples from the Dead Sea Transform: Tectonophysics, v. 445, p. 186 – 199.

Marco, S., Rockwell, T.K., Heimann, A., Frieslander, U., and Agnon, A., 2005, Late Holocene slip of the Dead Sea Transform revealed in 3D palaeoseismic trenches on the Jordan Gorge segment: Earth Planet. Sci. Lett., v. 234, p. 189-205.

Marco, S., Ron, H., McWilliams, M.O., and Stein, M., 1998, High-Resolution Record of Geomagnetic Secular Variation from Late Pleistocene Lake Lisan Sediments (Paleo Dead Sea): Earth Planet. Sci. Lett., v. 161, p. 145-160.

Marco, S., Stein, M., Agnon, A., and Ron, H., 1996, Long term earthquake clustering: a 50,000 year paleoseismic record in the Dead Sea Graben: J. Geophys. Res., v. 101, p. 6179-6192.

McClusky, S., Reilinger, R., Mahmoud, S., Sari, D.B., and Tealeb, A., 2003, GPS constraints on Africa (Nubia) and Arabia plate motions: Geophys. J. Int., v. 155, p. 126.

Meghraoui, M., Gomez, F., Sbeinati, R., derWoerd, J.V., Mouty, M., Darkal, A.N., Radwan, Y., Layyous, I., Najjar, H.A., Darawcheh, R., Hijazi, F., Al-Ghazzi, R., and Barazangi, M., 2003, Evidence for 830 years of seismic quiescence from palaeoseismology, archaeoseismology and historical seismicity along the Dead Sea fault in Syria: Earth Planet. Sci. Let., v. 210, p. 35-52.

Migowski, C., Agnon, A., Bookman, R., Negendank, J.F.W., and Stein, M., 2004, Recurrence pattern of Holocene earthquakes along the Dead Sea transform revealed by varve-counting and radiocarbon dating of lacustrine sediments: Earth and Planetary Science Letters, v. 222, p. 301-314.

Niemi, T.M., Zhang, H., Atallah, M., and Harrison, B.J., 2001, Late Pleistocene and Holocene slip rate of the Northern Wadi Araba fault, Dead Sea Transform, Jordan: Journal of Seismology, v. 5, p. 449-474.

Pe'eri, S., Wdowinski, S., Shtibelman, A., and Bechor, N., 2002, Current plate motion across the Dead Sea Fault from three years of continuous GPS monitoring: Geophys. Res. Lett., v. 29, p. doi: 10.1029/2001GL013879.

Quennell, A.M., 1956, Tectonics of the Dead Sea rift, Congreso Geologico Internacional, 20th sesion, Asociacion de Servicios Geologicos Africanos: Mexico City, p. 385-405.

Reches, Z., and Hoexter, D.F., 1981, Holocene seismic and tectonic activity in the Dead Sea area: Tectonophysics, v. 80, p. 235-254.

Reilinger, R., McClusky, S., Vernant, P., Lawrence, S., Ergintav, S., Cakmak, R., Ozener, H., Kadirov, F., Guliev, I., Stepanyan, R., Nadariya, M., Hahubia, G., Mahmoud, S., Sakr, K., ArRajehi, A., Paradissis, D., Al-Aydrus, A., Prilepin, M., Guseva, T., Evren, E., Dmitrotsa, A., Filikov, S.V., Gomez, F., Al-Ghazzi, R., and Karam, G., 2006, GPS constraints on continental deformation in the Africa-Arabia-Eurasia continental collision zone and implications for the dynamics of plate interactions: Journal of Geophysical Research-Solid Earth, v. 111, p. -.

Ron, H., Freund, R., Garfunkel, Z., and Nur, A., 1984, Block-rotation by strike-slip faulting: structural and paleomagnetic evidence: J. Geophys. Res, v. 89, p. 6256-6270.

Ron, H., and Levi, S., 2001, When did hominids first leave Africa?: New high-resolution magnetostratigraphy from the Erk-el-Ahmar Formation, Israel: Geology, v. 29, p. 887-890.

Rotstein, Y., Bartov, Y., and Frieslander, U., 1992, Evidence for local shifting of the main fault and changes in the structural setting, Kinarot basin, Dead Sea transform: Geology, v. 20, p. 251-254.

Salamon, A., Hofstetter, A., Garfunkel, Z., and Ron, H., 1996, Seismicity of the eastern Mediterranean region: Perspective from the Sinai subplate: Tectonophysics, v. 263, p. 293-305.

Shaliv, G., 1991, Stages in the tectonic and volcanic history of the Neogene basin in the Lower Galilee and the valleys: Geological Survey of Israel - Report (in Hebrew, English abstract), v. 11/91, p. 1–94.

Shamir, G., Eyal, Y., and Bruner, I., 2005, Localized versus distributed shear in transform plate boundary zones: The case of the Dead Sea Transform in the Jericho Valley: Geochemistry Geophysics Geosystems, v. 6, p. -.

Sneh, A., 1981, The Hazeva Formation in the northern Arava: Isr. Jour. Earth Sci., v. 30, p. 81-92.

—, 1982, Quaternary of the northwestern Arava, Israel: Isr. Jour. Earth Sci., v. 31, p. 9-16.

Stein, M., 2001, The sedimentary and geochemical record of Neogene - Quaternary water bodies in the Dead Sea Basin - inferences for the regional paleoclimatic history: Journal of Paleolimnology, v. 26, p. 271-282.

Steinitz, G., and Bartov, Y., 1986, The 1985 time table for the tectonic events along the Dead Sea transform: Terra Cognita, v. 6, p. 160.

ten Brink, U.S., Rybakov, M., Al-Zoubi, A.S., Hassouneh, M., Frieslander, U., Batayneh, A.T., Goldschmidt, V., Daoud, M.N., Rotstein, Y., and Hall, J.K., 1999, Anatomy of the Dead Sea transform: Does it reflect continuous changes in plate motion?: Geology, v. 27, p. 887-890.

ten-Brink, U.S., and Ben-Avraham, Z., 1989, The anatomy of a pull-apart basin: Reflection observations of the Dead Sea basin: Tectonics, v. 8, p. 333-350.

Tsatskin, A., and Nadel, D., 2003, Formation processes at the Ohalo II submerged prehistoric campsite, Israel, inferred from soil micromorphology and magnetic susceptibility studies: Geoarchaeology-an International Journal, v. 18, p. 409-432.

Wdowinski, S., Bock, Y., Baer, G., Prawirodirdjo, L., Bechor, N., Naaman, S., Knafo, R., Forrai, Y., and Melzer, Y., 2004, GPS Measurements of current crustal movements along the Dead Sea Fault: J. Geophys. Res., v. 109, p. 1-16.

Hula Valley

17.2.2009

Field leader

Amotz Agnon

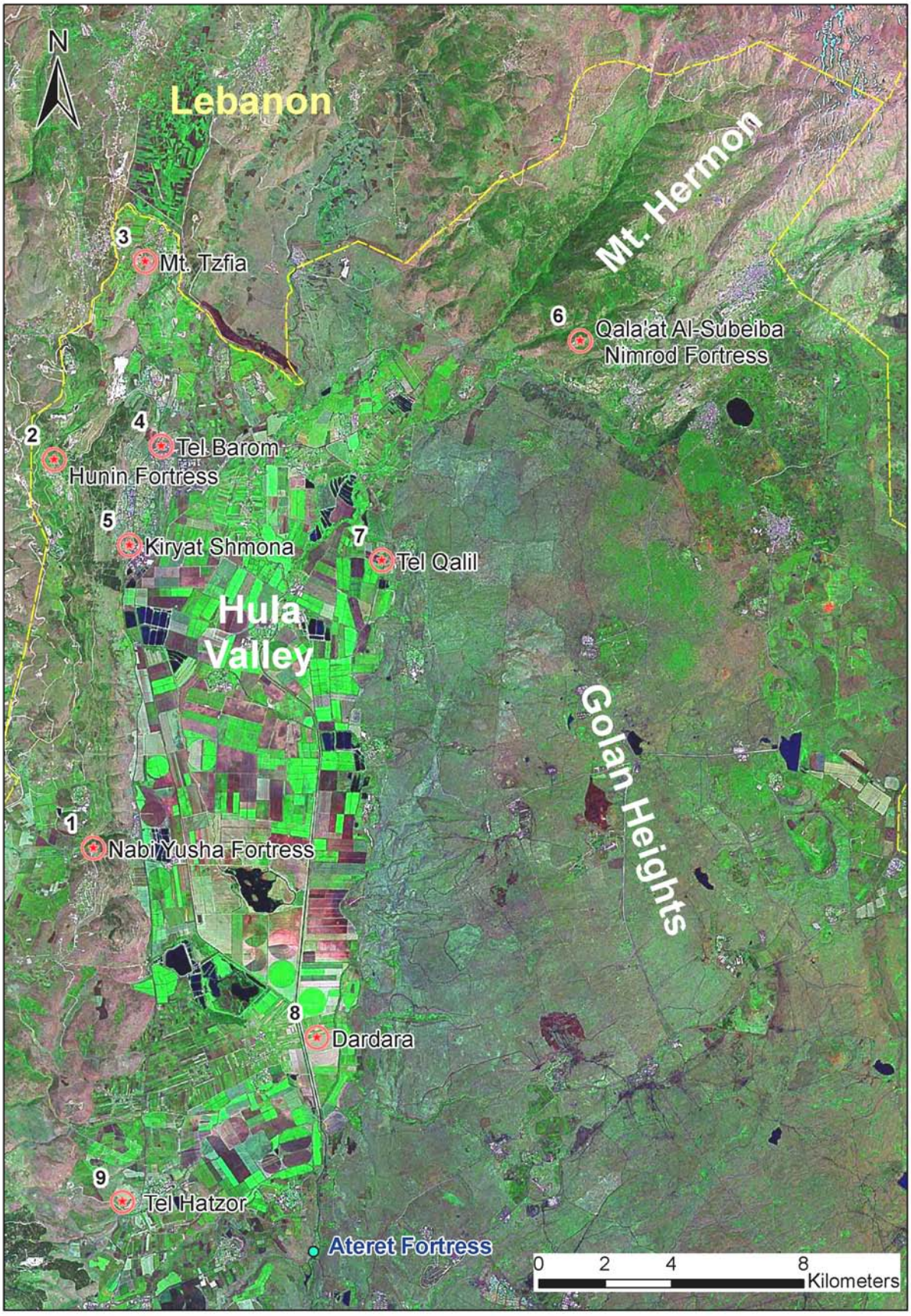
N
Lebanon
Mt. Hermon
3
Mt. Tzfia
6
Qala'at Al-Subeiba
Nimrod Fortress
4
Tel Barom
2
Hunin Fortress
5
Kiryat Shmona
7
Tel Qalil
Hula
Valley
Golan Heights
1
Nabi Yusha Fortress
8
Dardara
9
Tel Hatzor
Ateret Fortress
0 2 4 8
Kilometers

Hula basin

Field guides: Amotz Agnon[1], Hagai Ron[1], Mor Kanari[2], Benjamin Medvedev[3], Moshe Politi[1], Oded Katz[4], Shmuel Marco[2], Rivka Amit[4], Ariel Heimann[5]

[1]Institute of Earth Sciences, The Hebrew University of Jerusalem
[2] Department of Geophysics and Planetary Sciences, Tel Aviv University
[3]The Geophysical Institute of Israel
[4]Geological Survey of Israel
[5]The Davidson Institute of Science Education, Weizmann Institute of Science, Israel

amotz@cc.huji.ac.il

This field-trip will present the following a perspectives on the Hula basin (numbers preceded by # refer to stops given in detail below): the basin as a part of the regional framework, namely a pull-apart basin straddling a major branching point along the transform (#1,#3,#9); intense meso-structures imprinted in the pre-rift carbonates (#2); rockfalls from tectonic scarps (#4); detection of active strands in the shallow subsurface (#5,#8); seismic damage to Medieval Period monuments (#2;#6); subsidiary structures at the margins and trenching results (#7). The route is planned as a clockwise loop.

Background

The Hula and Marj Ayun basins are the northernmost of a string of elongated transform basins along the plate boundary from the Gulf of Aqaba in the south (Fig 1). The stratigraphic section exposed records transition from a carbonate platform on the southern margins of the Neo-Thetys (Jurassic to Paleogene) to a continental margin subject to Neogene to Quaternary rifting and volcanism (Fig. 2). The volcanic plateau field that bounds the Hula valley form east (Golan Heights) is the western edge of the active volcanic field Harrat a Shammah. Neogene to Pleistocene volcanism has affected the Galilee on the western margin of the Hula (Fig. 3) and contributed to the basin fill (Fig. 4). Dating drilled flows has enabled Heimann and Steinitz to constrain the rate of subsidence (Fig. 5). The marginal normal faults east and west of the valley dominate the topography, but a through-going fault is indicated in the short wave content of the gravity field and the epicenter locations (Fig. 6). The stops of the tours (#1 to #9) are shown on Fig. 7.

The Western Margin

We start with a breath taking vista of the Hula basin from the top of the cliff uplifted at the footwall of the western marginal fault (Nebi Yusha / Yesha fortress, #1). The mountain is around 400m above sea-level, whereas the depression below is around 70m (~1000 ft. difference). The shape of the valley contour (contact of fill and bedrock) is a parallelepiped with a sense inverted relatively to the expected for a left lateral transform (Figs. 8 and 10). This may be related to the

slip branched to the north east, and possibly to some shear partitioned to the south west. The branching point is hinted on the gravity map (Fig. 6) and old seismic lines are available to test this hypothesis (Fig. 9). Figs. 10 to 13 corroborate Schattner and Weinberger's (2008) suggestion for a through-going transform fault, and also our suggestion for branching close to the depocenter (Politi et al., 2008).

We follow the footwall block to Chastel Neuf / Kal'at Hunin (#2), a Crusader to Ottoman castle, located close on a splay of the Roum fault (a significant branch of the Dead Sea transform from the north-west corner of the basin to the Lebanese coast near Beirut). The castle was demolished three times by large seismic events (1202, 1759, 1837, the last one rupturing the Roum fault). The moat exposes severe tectonic deformation experienced by the bedrock before construction (Ron et al., 1997).

We descend to the valley to Har Tzfiyah (Mt. Vista - stop #3), where we observe the northwestern branching of the main fault to Yammouneh fault (major north-western branch), Roum fault (western north-west branch) and Hasbaya (eastern north-western branch) (Fig. 14).

Then we take a closer look at the transform near Tel Barom (#4), where a fault-zone-wave experiment shows a strong and narrow wave guide along the shallow hundreds of meters along the fault (Figs. 15-17). Fractured basalt exposed on a road cut may comprise the wave guide (Fig. 18). The fault juxtapose the basalt with marl that does not fracture (Fig. 19). We will see a campus constructed recently right on the main fault. Shtivelman et al. (2005) describe this experiment together with two similar surveys taken at Vadum Iacob / Ateret Casle, to be visited the next day, and near Eilat. We will see exposure of intensely fractured basalt that may act as a wave-guide. Tel-Barom turns out to be situated right on the main strand of the fault and a promising site for future archaeosesimic excavations.

The next stop (#5) features earthquake induced rockfalls and their dating, described below by Kanari et al.

The Eastern Margin

We cross the valley to the east passing by numerous archeological sites with their rich archaeoseismic potential yet to be realized (Tel Dan, Tel Banyas, to name the most famous) (Fig. 7). We ascend nearly 700m to Kal'at A-sSubeiba / Nimrod fortress to observe the muslim monuments damaged heavily by the 1759 seismic events (#6). We will study the shifted arches and vaults that record the direction of shaking. On the way south we visit the eastern scarp at the local push-up Tel Qalil (#7), near the paleoseismic trench site of Azaz fault (Zilberman et al., 2000) (Fig. 14).

The Historical Lake and the Southern Depression

Stop #8 is on the lake bed, as testified by the mollusk shells abundant in the agricultural soil. This is the site of a high resolution seismic/gravity study that features a positive flower structure up to several tens meters below the surface (Fig. 20). This survey corroborates the location of the through-going fault suggested by Schattner and Weinberger (2008). A trench excavated lake

sediment poor in datable material (Medvedev et al., 2008). Intense fracturing has been identified and future work will focus on finer geophysical imaging and better age control.

Stop #9 will give us a last view of the depression from Tel Hatzor, a biblical ruin of a major city.

References

Belitzky, S., 2002. The morphotectonic structure of the lower Jordan Valley – an active segment of the Dead Sea Rift, EGU Stephan Mueller Special Publications Series vol. 2, pp 95-103.

Freund, R., Garfunkel, Z.,1976. Guidebook to excursion along the Dead Sea Rift. Dept. Geol., Hebrew Univ. Jerusalem, 27 p.

Heimann, A., Ron, H., 1987. Young faults in the Hula pull-apart basin, central Dead Sea transform, Tectonophys., 141, 117-124.

Heimann, A., Ron, H., 1993. Geometric changes of plate boundaries along pat of the northern Dead Sea transform: chronologic and paleomagnetic evidence, Tectonics, 12, 477-491.

Heimann, A., Steinitz, G., 1987. K-Ar dating of the Ramat Korazim basalts, Dead Sea Rift, Israel Geological Society, annual meeting; abstracts, 54-56.

Heimann, A., Steinitz, G., Mor, D., Shaliv, G., 1996. 40Ar/ 39Ar total gas ages of basalts from Notera 3 well, Hula Valley, centrl Dead Sea Rift: stratigraphic and tectonic implications. Isr. J. Earth Sci., 38,173-184.

Medvedev, B., Makovsky, Y., Agnon, 2008a. A.Slip partitioning in the Hula Basin: new evidence from high resolution geophysics, Israel Geological Society, annual meeting; abstracts, 65.

Medvedev B., Makovsky,Y., Bergman, N., Agnon, A., 2008b. Multi-scale fault imaging in the Hula basin, Northern Israel, EOS Trans. AGU, 89,Fall Meet. Suppl.,cAbstract NS13A-1083

Politi, M., Medvedev, B., Shamir, G., Makovsky, Y., Agnon, A, 2008. Branching of the Dead Sea Transform at the Hula Basin; evidence from the sub-surface, srael Geological Society, annual meeting; abstracts, 78.

Ron, H., Shamir, G., Eyal, M. 1997. Deformation of Margaliot block between Roum and Margaliot faults. Isr. Geol. Soc. Annu. Mtg., Kefar Gil'adi, Field trip Guide- book, pp. 33–45 (in Hebrew).

Rybakov, M., Fleischer, L., ten Brink, U., 2003. The Hula valley subsurface inferred from gravity data. Isr. J. Earth Sci., 52, 113-122.

Schattner U., Weinberger R., 2008. A mid-Pleistocene deformation transition in the Hula basin, northern Israel: Implications for the tectonic evolution of the Dead Sea Fault, Geochem. Geophys. Geosyst. 9, Q07009.

Shamir, G., Feldman, L., 1996. Earthquake activity in the Qiryat-Shmemona area, The geophysical Institute of Israel, Rep. # 953/160/96.

Shtivelman, V., Marco, S., Reshef, M., Agnon, A., Hamiel, Y., 2005. Using trapped waves for mapping shallow fault zones, Near Surface Geophys., 3, 95-101

Sneh, A., Weinberger, R. 2004. Geology of the Metulla quadrangle, northern Israel: Implications for the offset along the Dead Sea Rift. Isr. J. Earth Sci. 52, 123–138.

Zilberman E., Amit R., Heimann A., Porat, N., 2000. Changes in Holocene Paleoseismic activity in the Hula pull-apart basin, Dead Sea Rift, northern Israel, Tectonophys., 321,237-252.

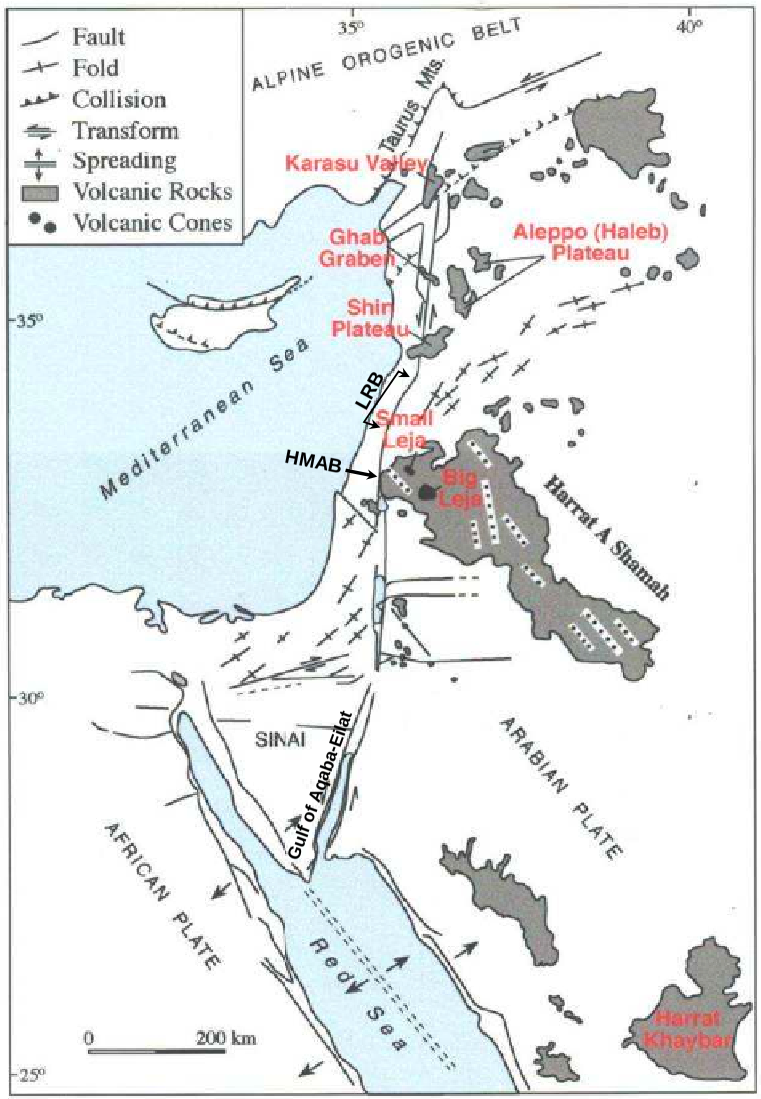

Figure 1: General tectonic setting of Israel and adjacent areas including the volcanic fields (Heimann et al., 1996, after Freund and Garfunkel, 1976). HMAB - Hula - MarjAyun basins. LRB: Lebanon restraining bend.

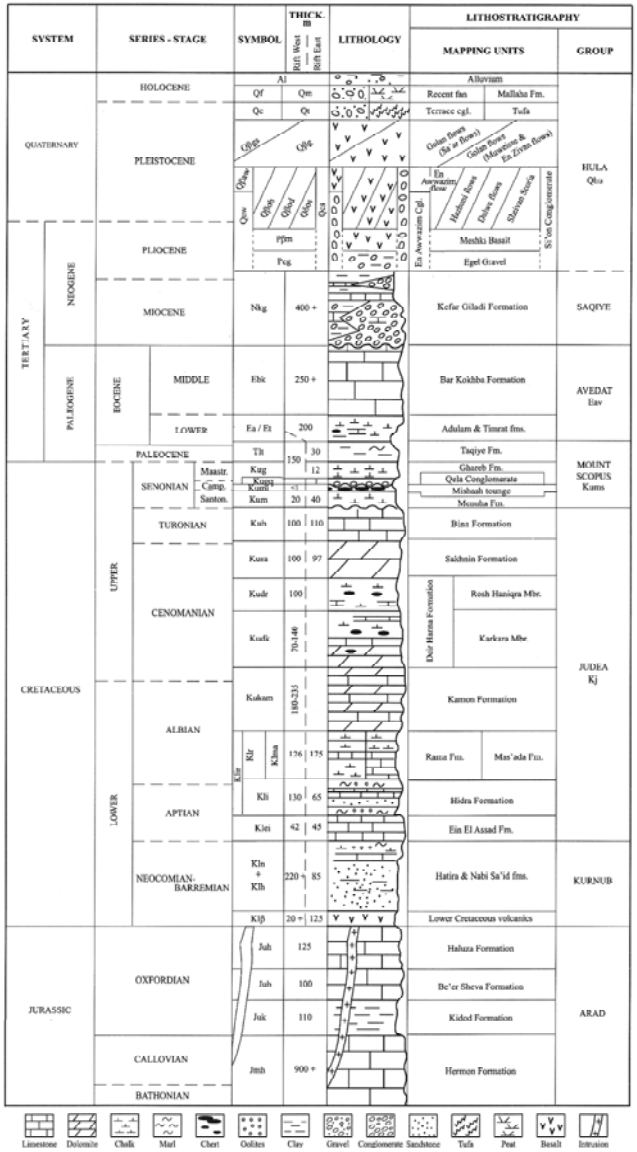

Figure 2: Stratigraphic section of rock units exposed in the Metula quadrangle which straddles the northern Hula valley. Sneh and Weinberger, 2004.

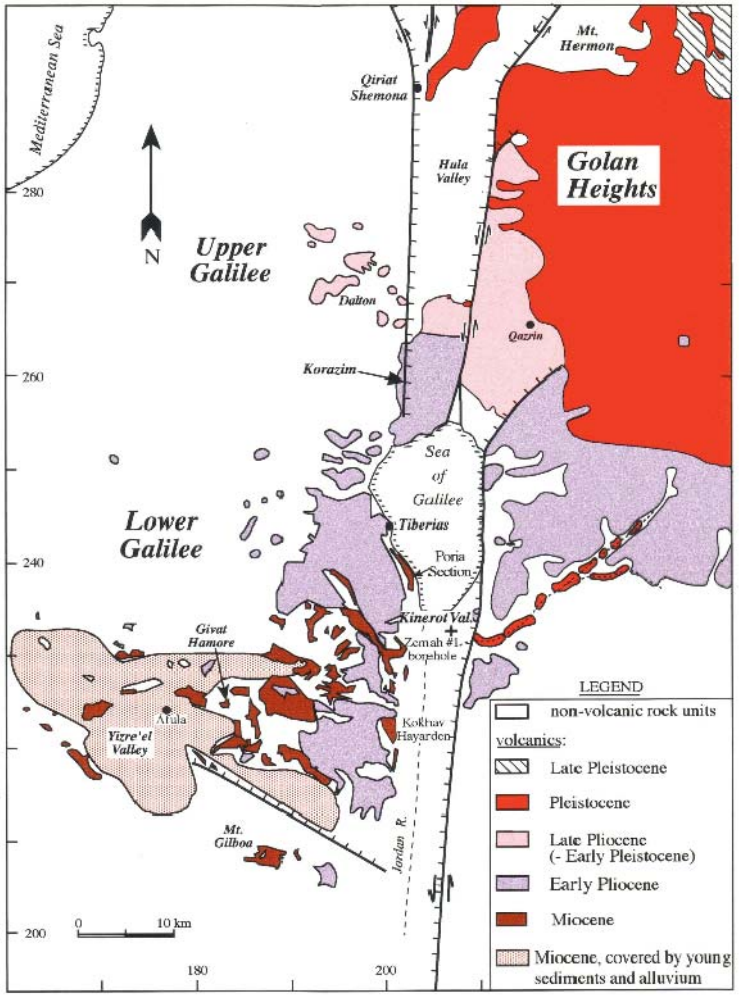

Figure 3: Cenozoic volcanism in the Galilee, northern Dead Sea Transform and the Golan (Heimann et al., 1996).

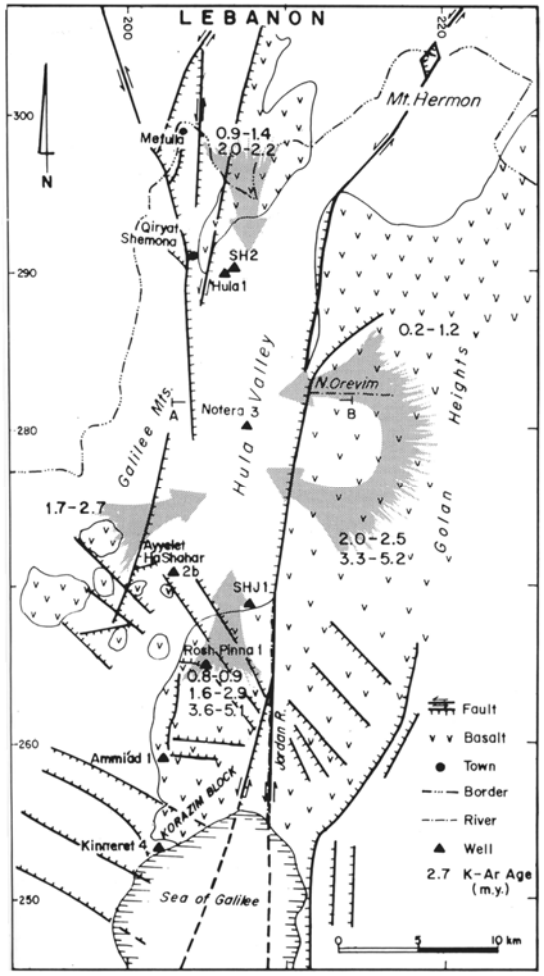

Figure 4: The possible sources of Plio-Pleistocene basalt flows found at the Hula Valley (surface and sub-surface) (Heimann and Steinitz, 1989).

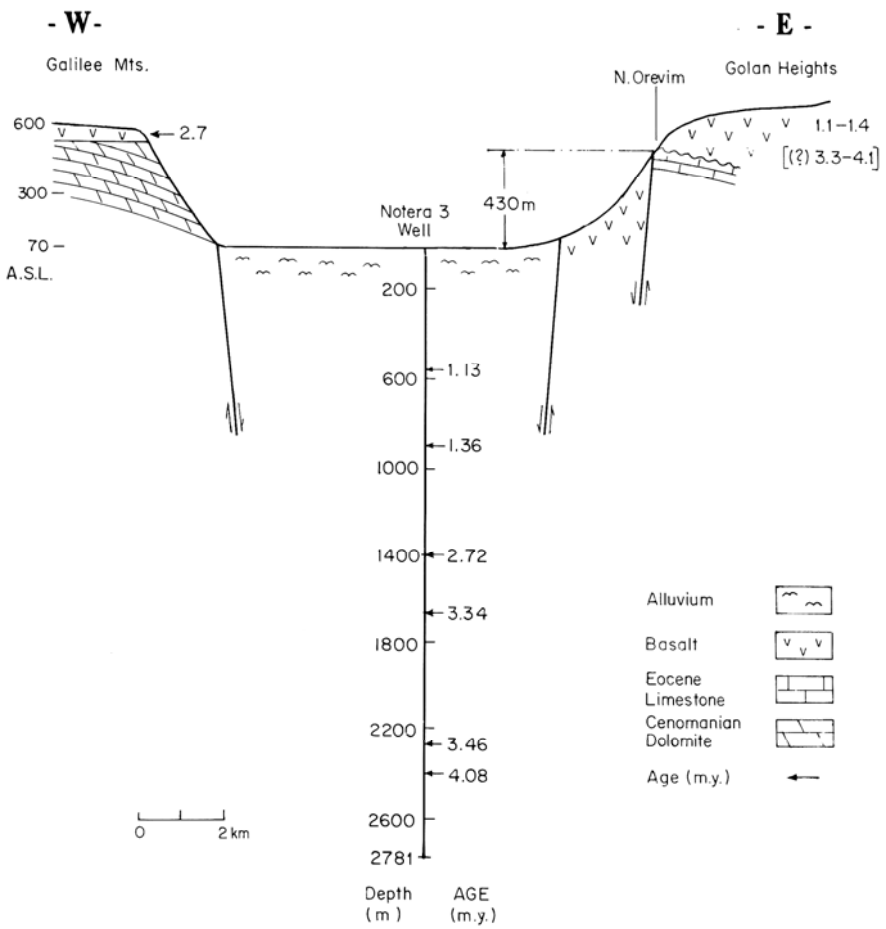

Figure 5: A schematic cross secttion through the Notera-3 well with K-Ar ages of basalt flows (Ma). Calculated subsidence rate are between 0.5 and 0.8 mm/yr (Heimann and Steinitz, 1989).

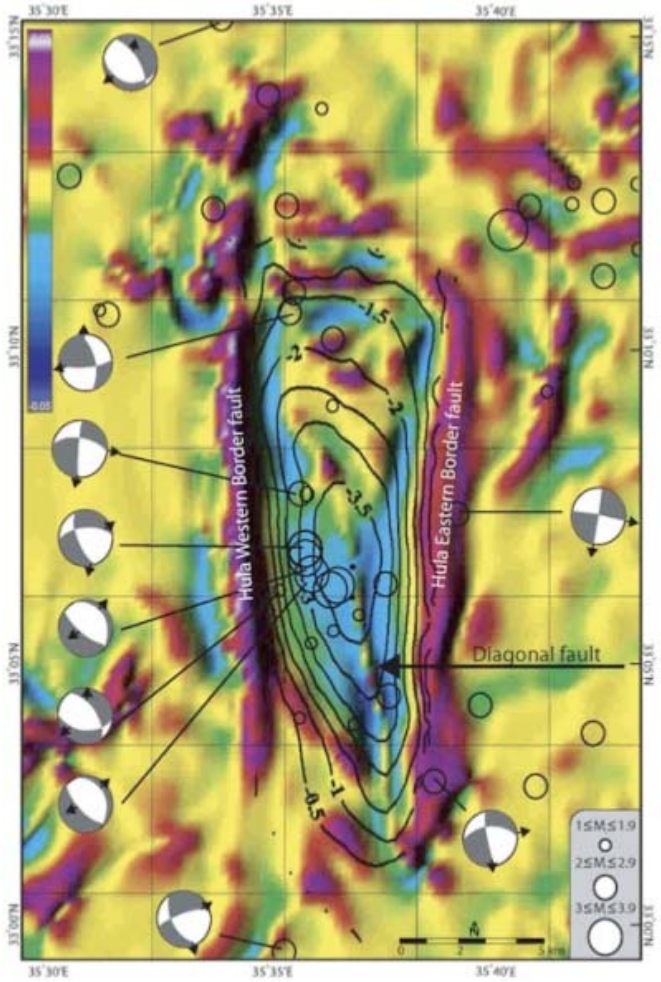

Figure 6: Dip curvature, second derivative of the gravity field superposed by structural 0.5 km contours of the base of the Hula basin fill (after Rybakov et al. 2003). Location of selected seismic events and focal plane solutions of earthquakes recorded between 1982 and 1997 (after Ron et al. 1997) are marked. Schattner and Weinberger (2008) identify the through going lineament with the main active strike-slip strand.

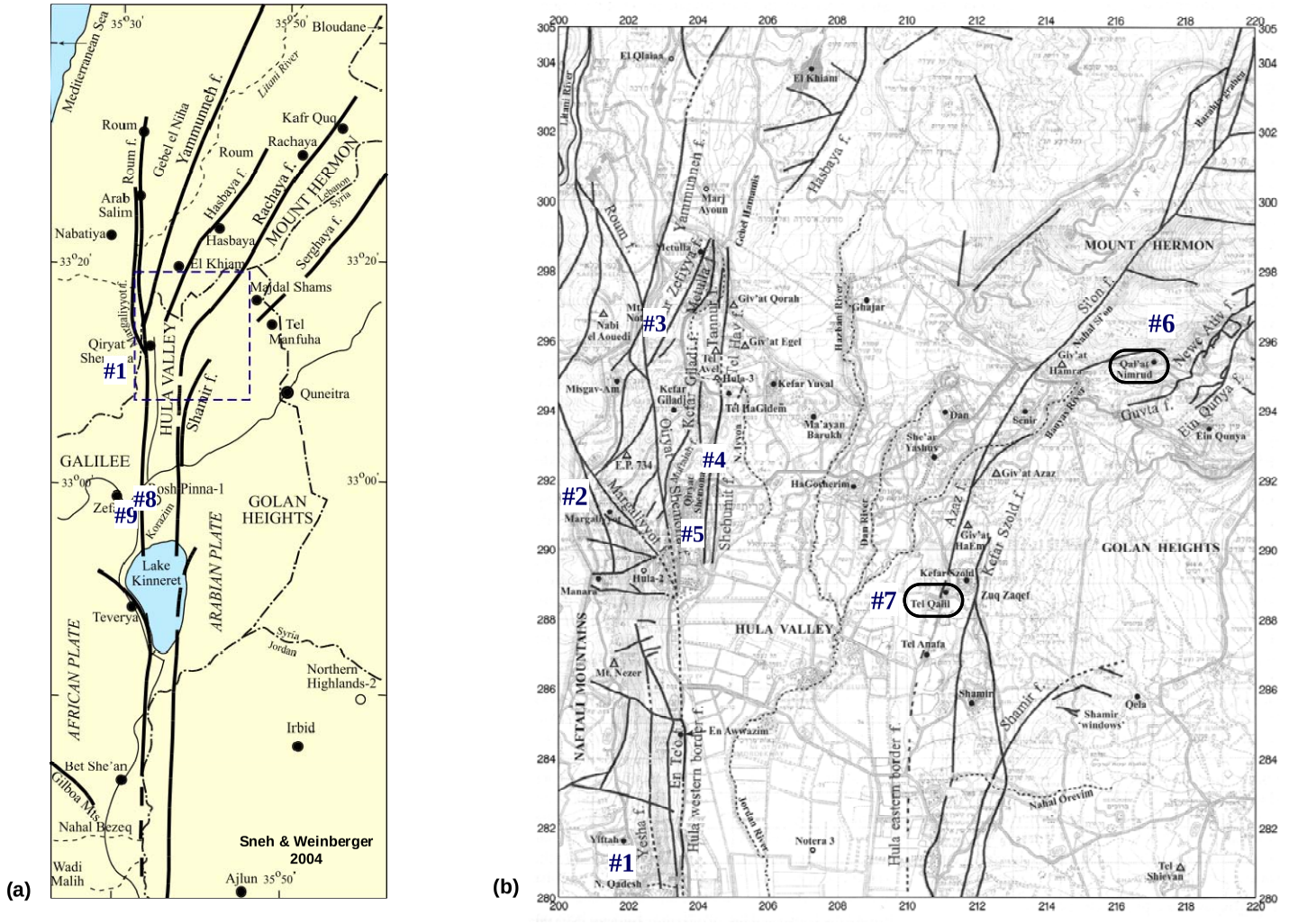

Figure 7: (a) A generalized tectonic map of the northern valleys. The first and last stops (#1, #8, #9) are shown. The broken-line quadrangle demarcates the location of the bottom figure.
(b) Excursion stops #2-#7 shown on a detailed fault map of Metulla quadrangle, Geological Map of Israel 1:50,000, GSI (Sneh and Weinberger, 2004).

Geologic map

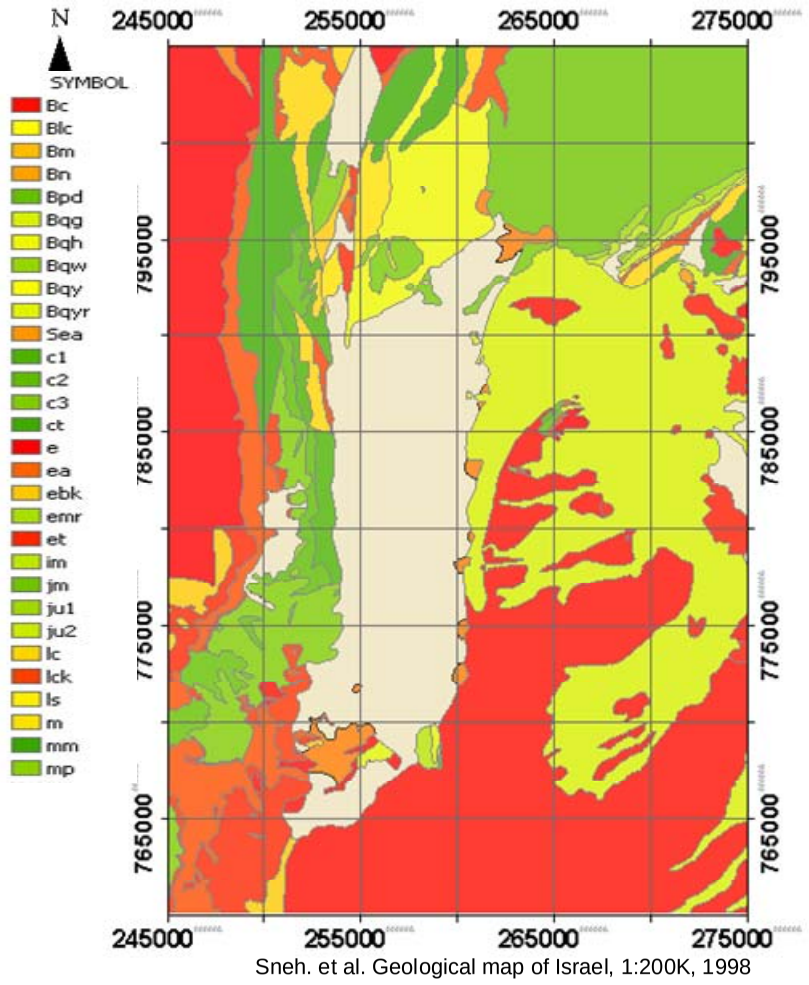

Figure 8: A geological map of the Hula basin. Note the "inverted" parallelepiped shape of the basin fill. Green shades - Upper Cretaceous (shallow marine); Orange - Paleogene (shallow marine); Yellow: Neogene (fluvial); Red: Plio-Pleistocene (volcanic); Grey: Late Quaternary (soil and clastic fill).

Seismic profiles and wells location

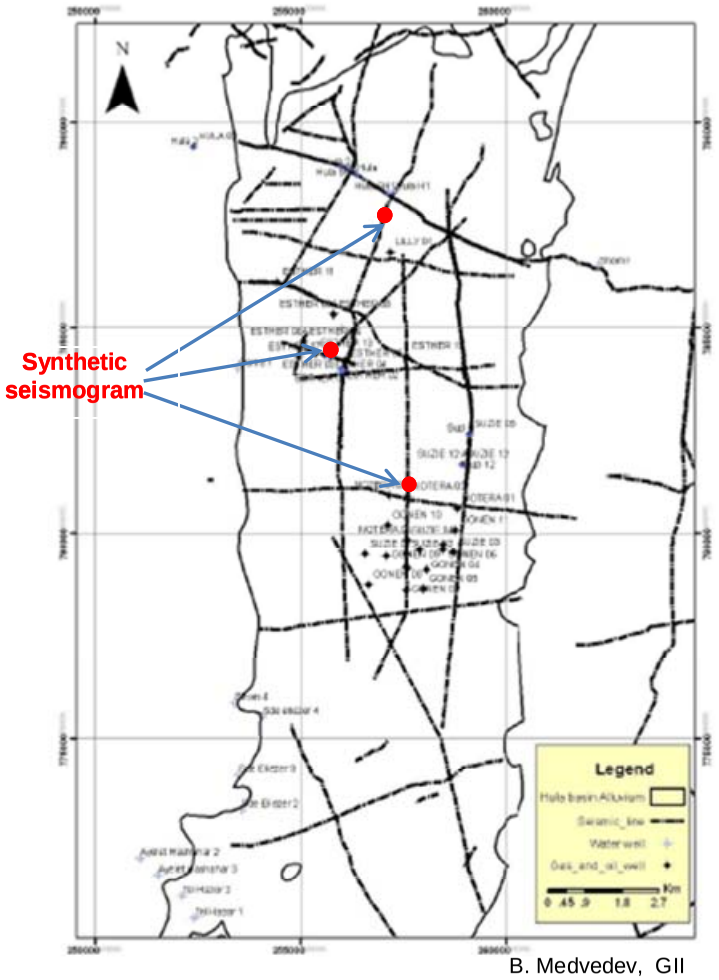

Figure 9: A map of seismic lines and wells in the Hula basin.

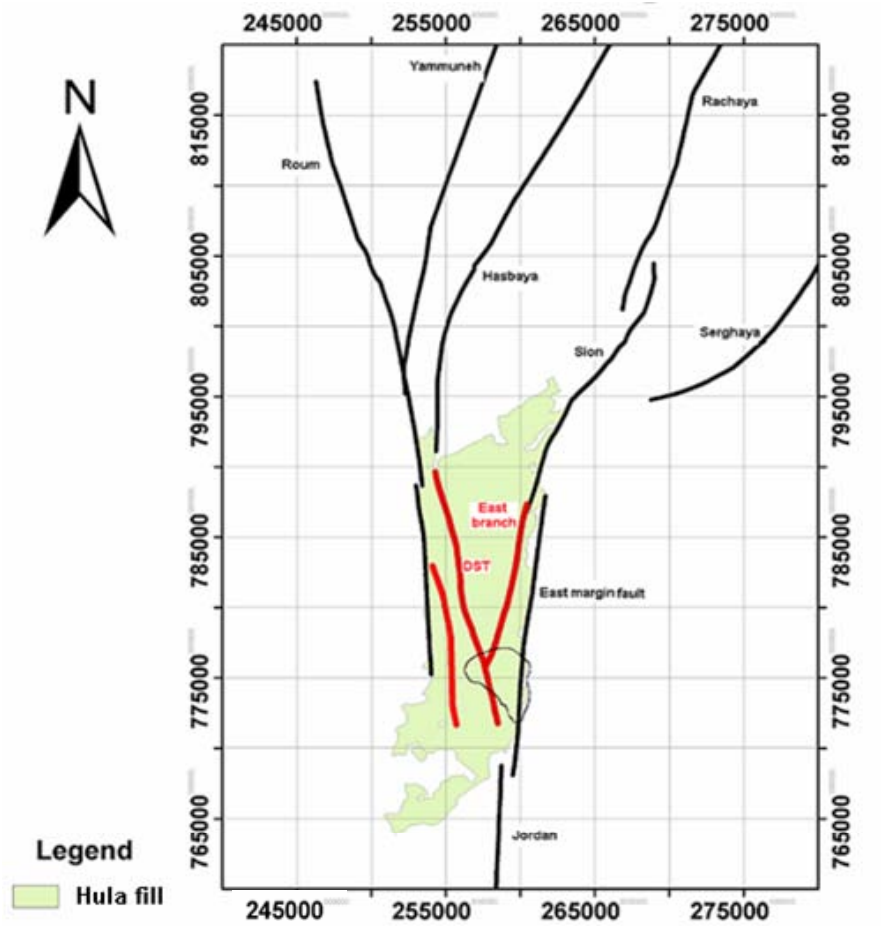

Fig. 10: Branching of DST. Faults – modified after, Heimann and Ron (1993), Shamir and Feldman (1996), Belitzky (2002), Sneh and Weinberger (2004) – Black Faults inferred from seismic – Red Hula basin fill – Green. ("inverted" parallelepiped).

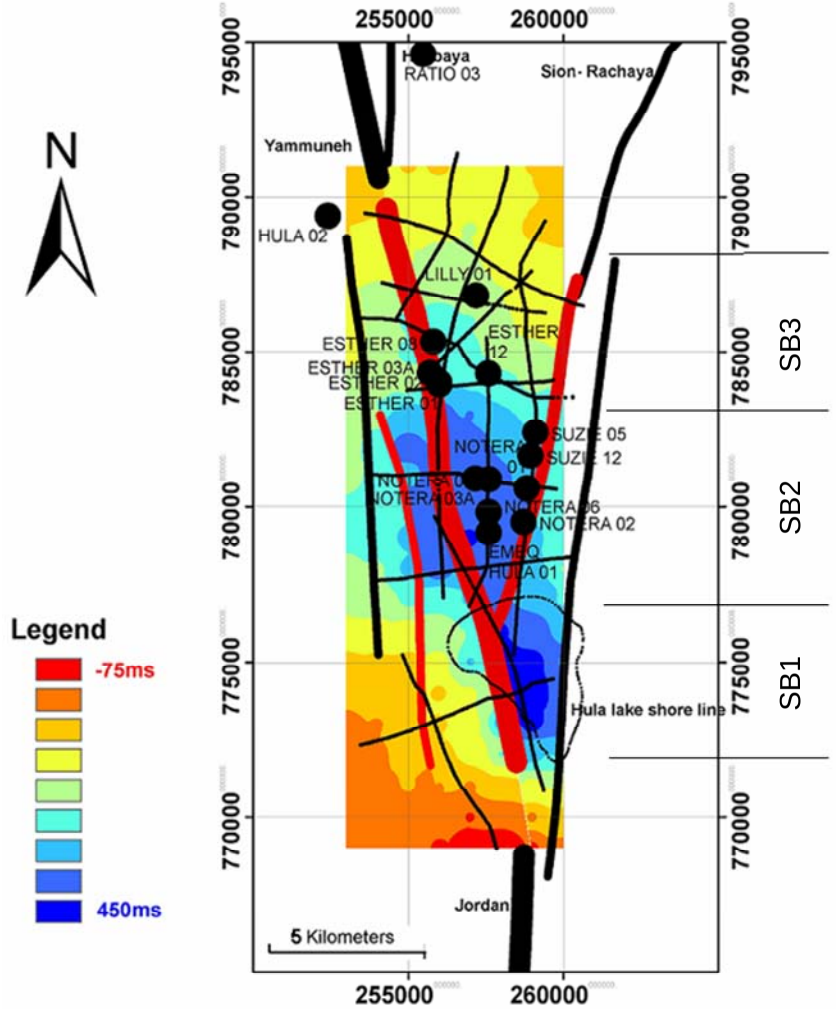

Fig. 11: A structural map (time) on top Ortal flows. An elongated depression along the eastern side of the main fault divided into 3 sub-basins. The sub-basins apparent east of the master fault: SB(1) - the recent depocenter correlating with the historical Hula lake (drained during the early 1950's), SB(2) - a central depression, bounded on either side by two main branches of the rift. SB(3) - a shallow sub-basin. See seismic profiles.

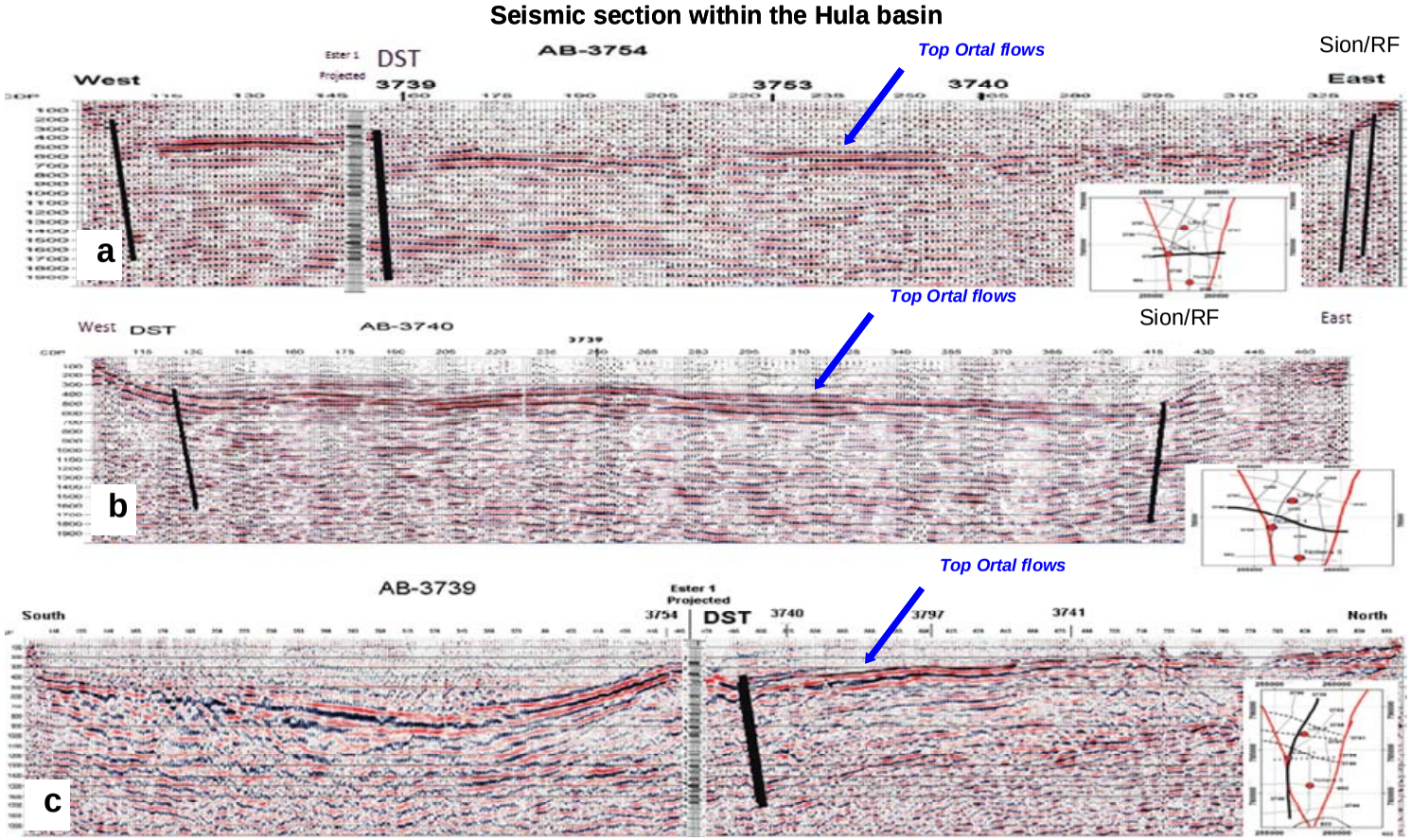

Fig. 12: Reprocessed seismic profiles (stack) after crooked line adjustments (B. Medvedev). Top Ortal basalt flows is prominent regional reflection character and amplitude. Ester 1 control borehole is shown in two of the lines for correlation.

a. 3754 line: E-W profile showing from left to right: (1) The exposed boundary western fault. (2) The master fault near Ester 1 well. (3) an eastern branch, hardly expressed at the surface.

b. 3740 line: E-W profile showing both the master fault and the eastern branch.

c. 3739 line: N-S profile showing the Ester structure near the master fault, Ester 1 borehole and the main depression southward.

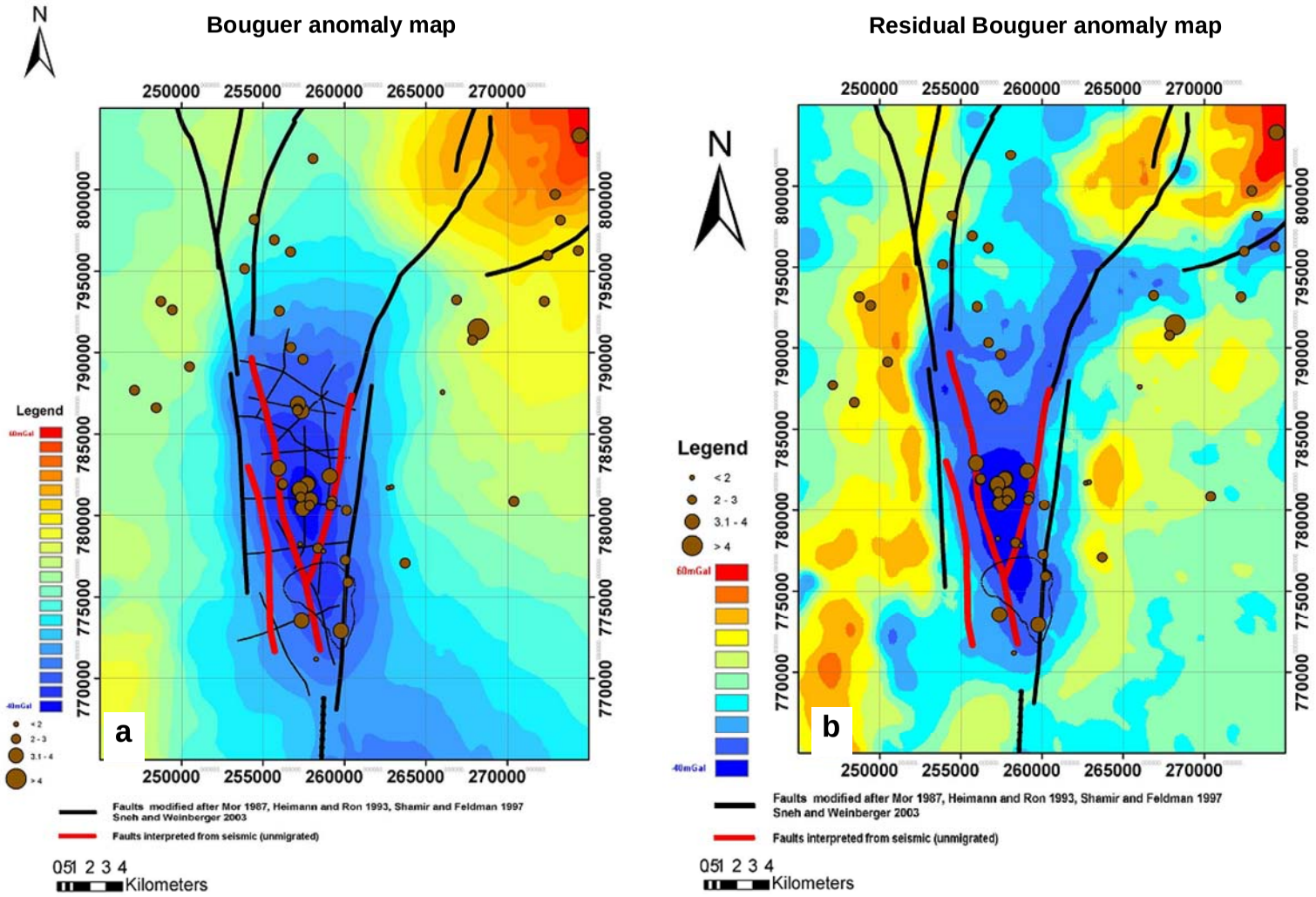

Fig. 13: Gravity maps.
a. Bouguer anomaly map with fault traces and relocated epicenters (courtesy of T. Meirov, GII) and seismic profiles.
b. Residual Bouguer anomaly map showing the main depression and the DST branches.

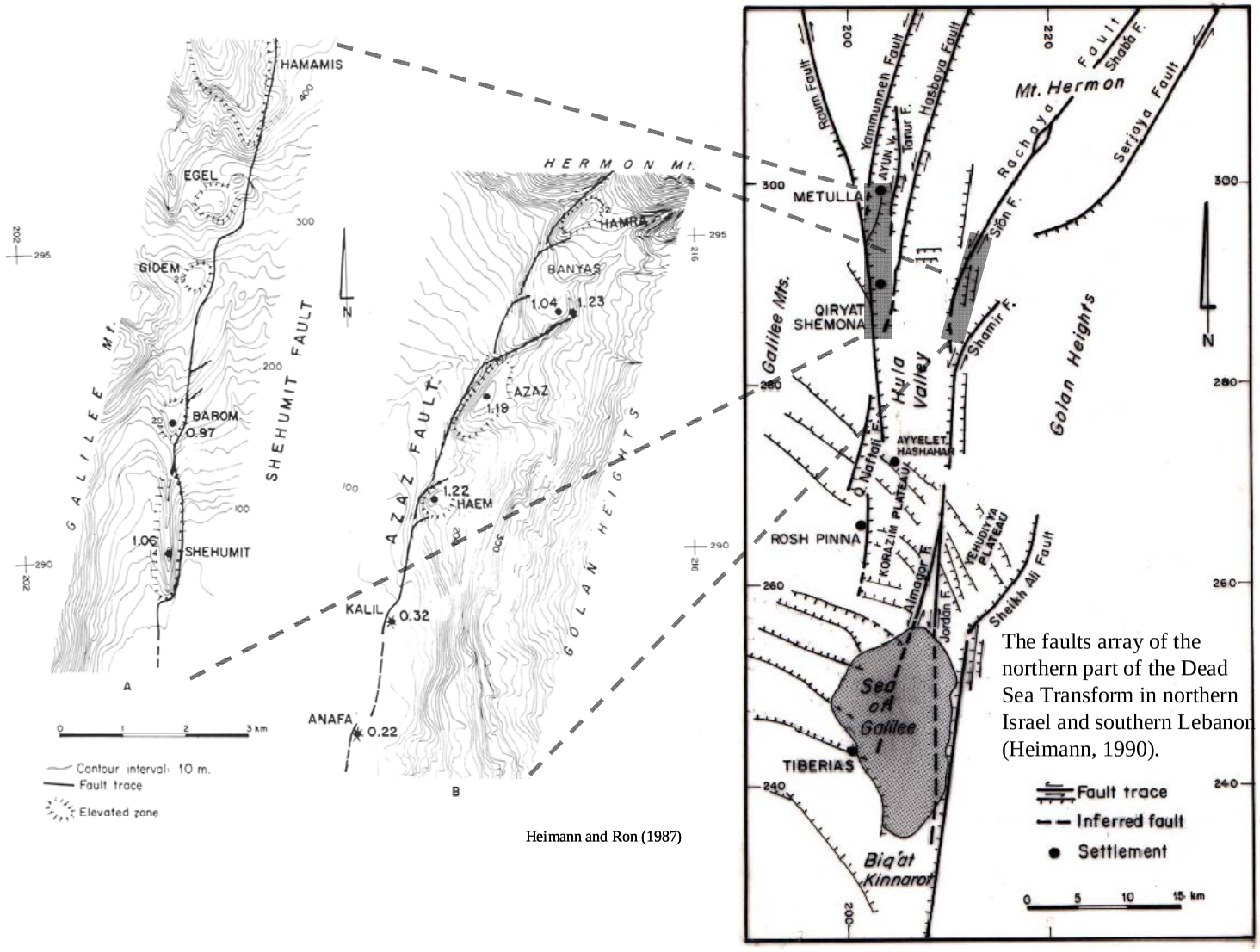

The faults array of the northern part of the Dead Sea Transform in northern Israel and southern Lebanon (Heimann, 1990).

Figure 14: Active strands of the Dead Sea transform and related subsidiary strucures.

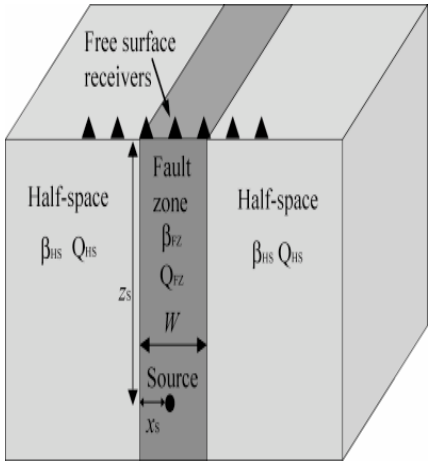

Figure 15: Output of fault-zone wave experiemnt at Tel-Barom (Stop #4). The seismograms show common shot gathers, no gain. Note that some of the shots show distinctive ringing at geophones around #20 after 400 ms. The schematic block on the left, depicts the experimantal layout (Shtivelman et al., 2005).

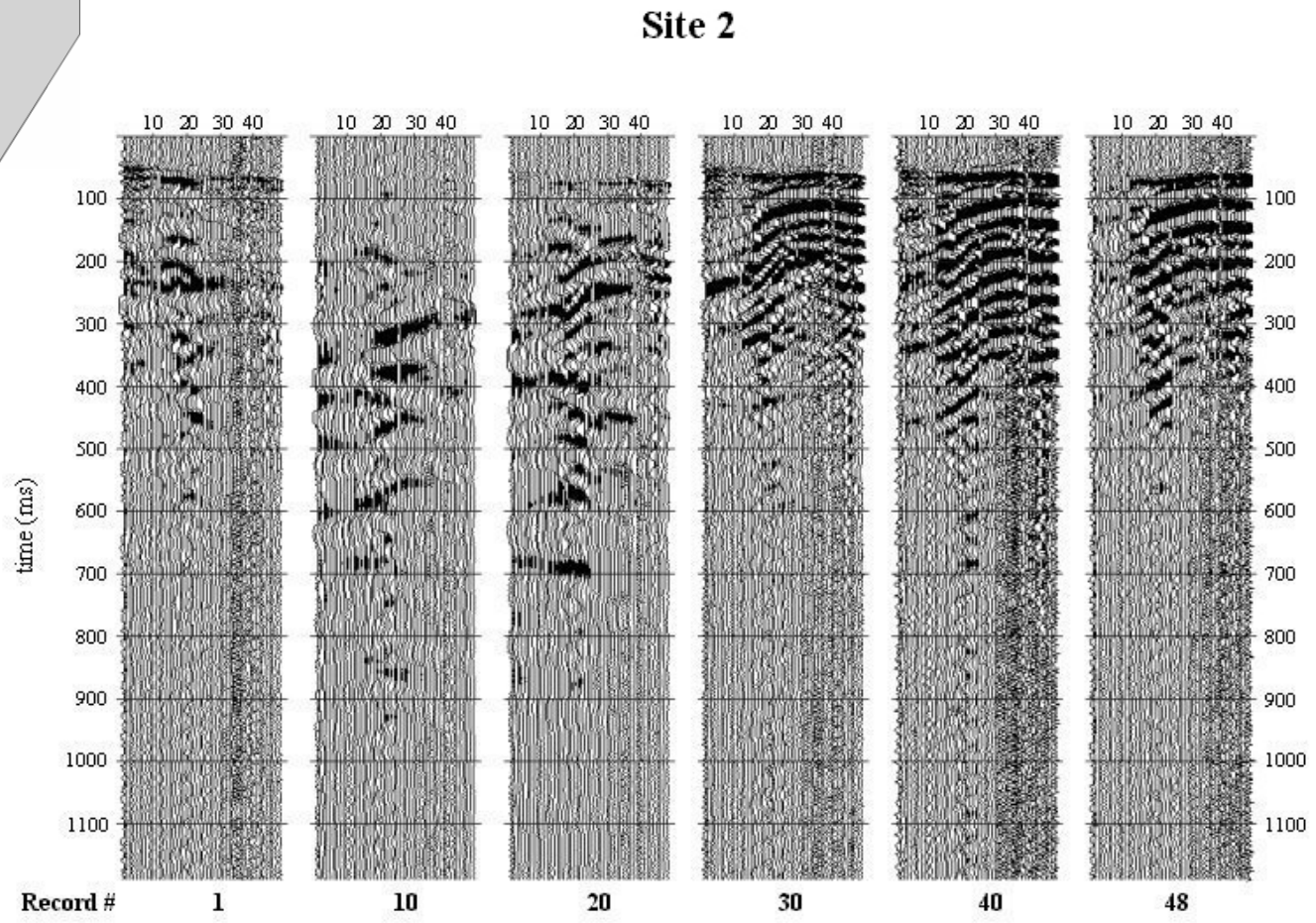

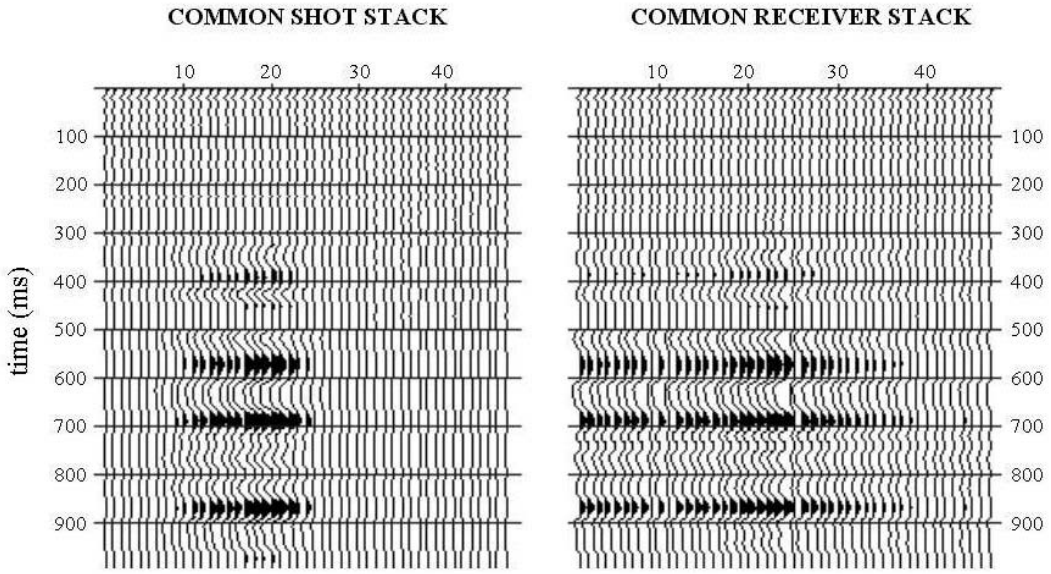

Figure 16: Stacks show cancelation of most of the arrivals before 400 ms, highlighting the fault zone waves. Waves from shots 10-24 (and mostly 15-21) are guided to recievers up to around 30, with a concentration around 20 (Shtivelman et al., 2005)

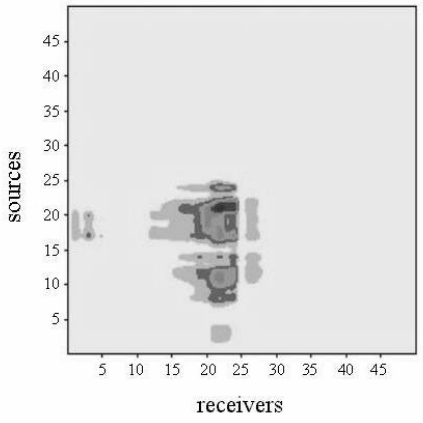

Figure 17: Energy map showing the preferred transfer of seismic energy between shots 16-20 and receivers 20-24, which is were the fault are located (Shtivelman et al., 2005).

Figure 18: A photo showing a Peistocene Basalt exposed at Tel-Brom, several hundred meters due south of the seismic experiment. The Basalt, juxtposed against Paleocene marle, is highly fractured near the fault, with the localized lower seismic speed presumably generating the wave-guide. location marked by star in the adjoined map.

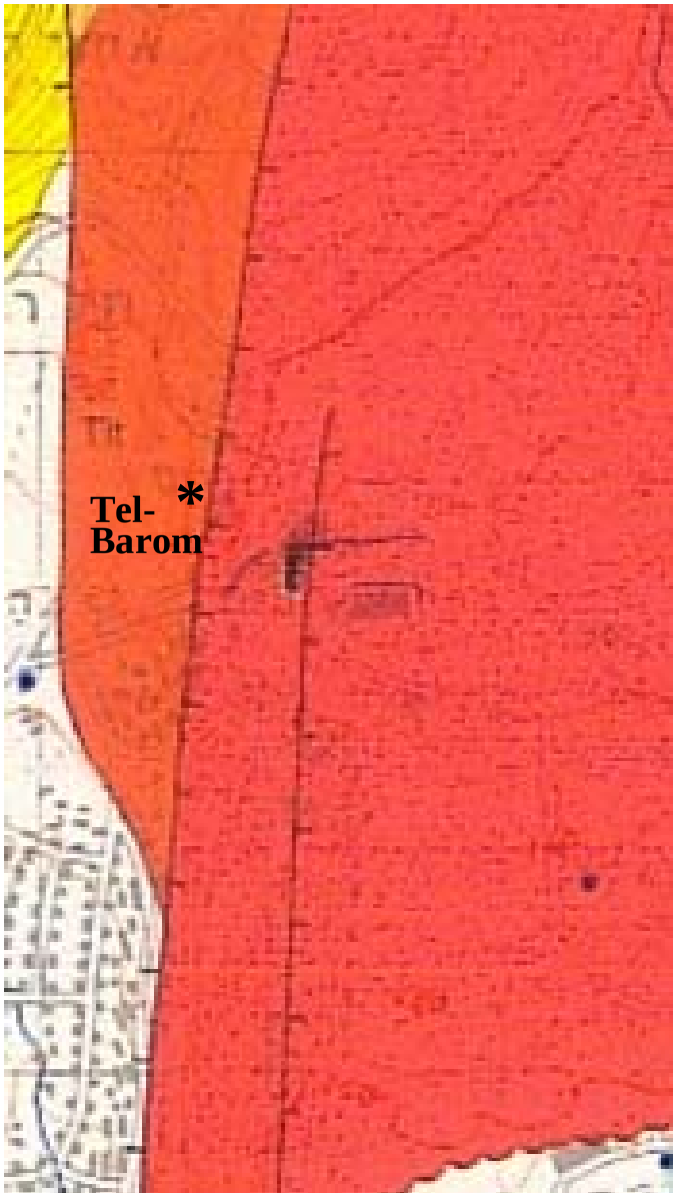

Figure 19: An excerpt from the geological Map of Metulla, Sneh and Weinberger, 2004. Orange - Paleocene Taqiya Formation. Yellow - Neogene Kfar Giladi Conglomerate. Red - Pleistocene Hasbani Basalt The light triangle marks the FZW active seismic experiment.

Figure 20: A high resolution geophysical survey (gravity and seismic profile as well as a fan-shooting experiment); (top) Layout on an airphoto; (bottom) A high resolution seismic profile. This profile shows detailed information to a depth of about 250m. A positive flower structure of 120m width is seen with several secondary faults merging to a single major fault at depth. Medvedev et al., 2008.

Evaluation of rockfall hazard to the city of Qiryat Shemona, N. Israel – possible correlation to earthquakes

Mor Kanari[1*], Oded Katz[2], Naomi Porat[2], Ram Weinberger[2], Shmuel Marco[1]

[1] Department of Geophysics and Planetary Sciences, Tel-Aviv University

[2] Geological Survey of Israel

kanarimo@post.tau.ac.il

* Field guide

The study estimates rockfall hazard for the town of Qiryat-Shemona, N. Israel, situated within the Dead Sea Transform fault system, at the foot of the Ramim cliff (Fig.1). The 40-m-thick Ein-El-Assad Formation limestone outcrops provide a source material for rock blocks (Fig. 2). Aerial photos from 1946–1951 show boulders of volume that range in between 1 m^3 and 150 m^3 situated within the now built town premises (Fig. 1). The study examines: (a) what are the properties of the source rock and what is the triggering mechanism? (b) which are the feasible downhill trajectories of the blocks and where do blocks stop? (c) when did rockfalls occur and what is the estimated recurrence interval? (d) what is the rockfall hazard, and what may be recommended as a mitigation design for Qiryat-Shemona?

To answer these questions hundreds of rock-blocks were mapped on the slopes above Qiryat-Shemona using both field surveys and aerial photos and their volume and spatial distributions are analyzed; burial ages of soil samples from beneath large fallen blocks were determined by OSL; rockfall trajectories were simulated using a commercial program (CRSP v4). Hazard evaluation maps for Qiryat-Shemona were compiled from the results of rockfall simulations. Simulated analyses of block velocity and kinetic energy may be used as parameters for the design of mitigation of rockfall damage for Qiryat-Shemona. Rockfall hazard estimation is derived from: a. rockfall recurrence time based on OSL age determinations; b. block size probability derived from block volume distribution.

Results show that the block volume distribution follows an exponential function of the form ax^b with b value –1.17, in agreement with worldwide rockfall inventories. OSL dating of 8 soil samples demonstrate clustering around dates that coincide with known earthquakes, historic and prehistoric (Fig. 3). It is concluded that earthquakes of large magnitudes (Mw≥7) are the triggering mechanism of rockfalls, yet apparently the rock-mass has to be weakened by joints and fractures to facilitate rockfalls. Maps of maximal downhill block travel distances combined with slope morphological analysis were used to suggest possible trajectories of downhill historical rockfalls. The simulation program variables are calibrated and later used to simulate possible downhill rockfall block trajectories towards the town premises. Simulation results are used to compile the rockfall hazard maps (Fig. 4).

It is concluded that at the south-westernmost part of town, life and property are at rockfall hazard in particular areas. Rockfall recurrence interval and probability of block volumes determined from the volume distribution yield hazard evaluation for the area of Qiryat-Shemona. OSL age analysis of rockfall events (850 years recurrence time and assuming that the last rockfall triggered by the 1202 AD earthquake) lead to a 6.5% probability for the next rockfall to occur within the next 50 years, and a 57% probability within the next 475 years. Evaluated rockfall hazard probability for 50 years is 0.044–0.065, and for 475 years 0.385–0.575, for block sizes or smaller than 10–125 m^3 respectively. Simulated results of block velocity and kinetic energy at specific impact locations on town yield block velocities of 10–15 m/s and kinetic energy of 18,000–45,000 kJ (98% confidence) for block volume of 125 m^3. The recommendation for environmental friendly rockfall damage mitigation design is forestation of the slope.

References

Kagan, E. J., Stein, M., Bar-Matthews, M., Agnon, A., 2007, A tale of two cataclysmic-earthquakes: 39 and 52 kyr BP, DST, Israel; a multi-archive study. AGU, Fall Meeting 2007, San Francisco, Session T12.

Yagoda-Biran, G., 2008, Seismic hazard estimation along the Eastern Margins of Sea of Galilee by back analysis of seismically induced natural and structural failures. MSc Thesis GSI/02/2008 90, p.

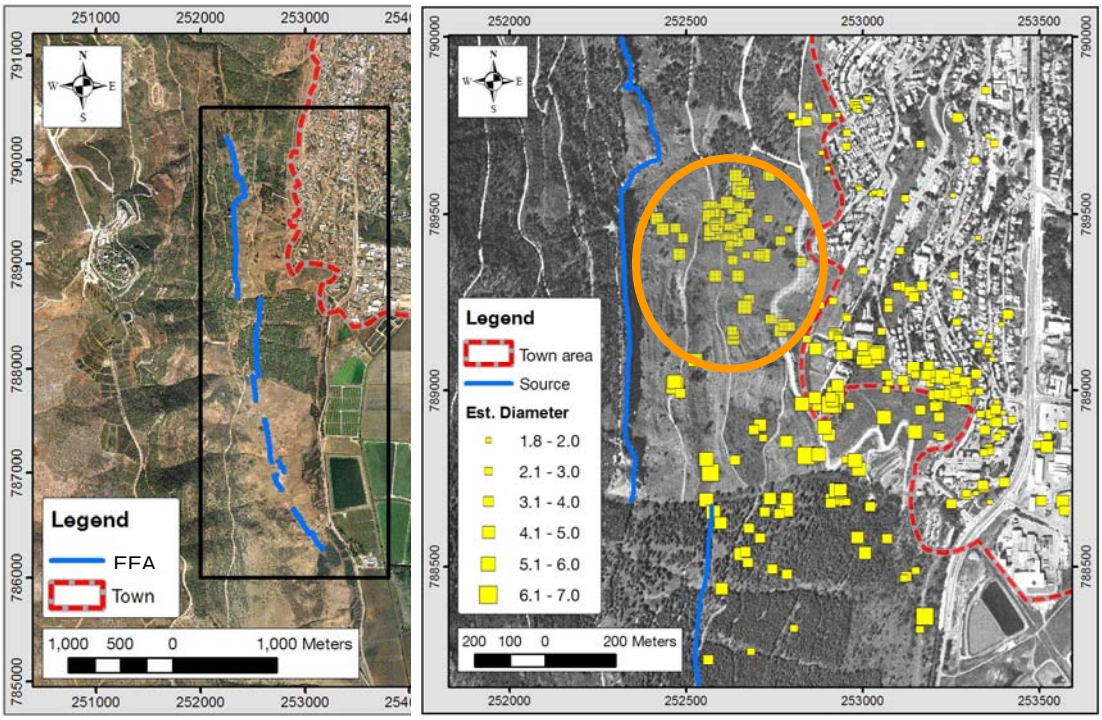

Figure 1: Left: Map of the study area in black rectangle. Ein-El-Assad Formation (EEA) is marked by blue line; town area in red dashed line. Right: location and estimated diameters of non-mappable blocks (located using 1946-51 aerials; blocks in orange ellipse used for the correlation between the sizes of field and non-mappable blocks.

Figure 2: Overview of the study area facing west towards the Ein-El-Assad outcrop. The rockfall talus in front. A normal fault at the rock mass can be observed on the top-right (yellow arrow): the overriding block on the right (north) is lower than the block to the left (south). A scar (yellow ellipse) in the outcrop, possibly the origin of rockfall mass, is clearly visible left (south) to the fault location.

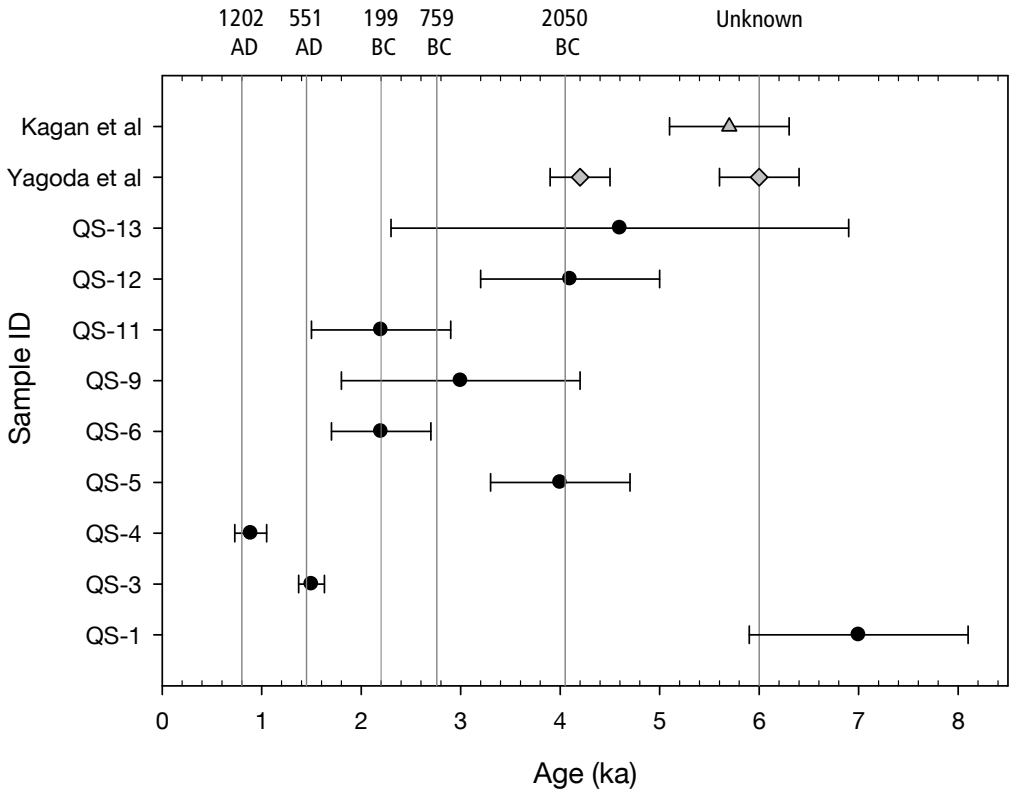

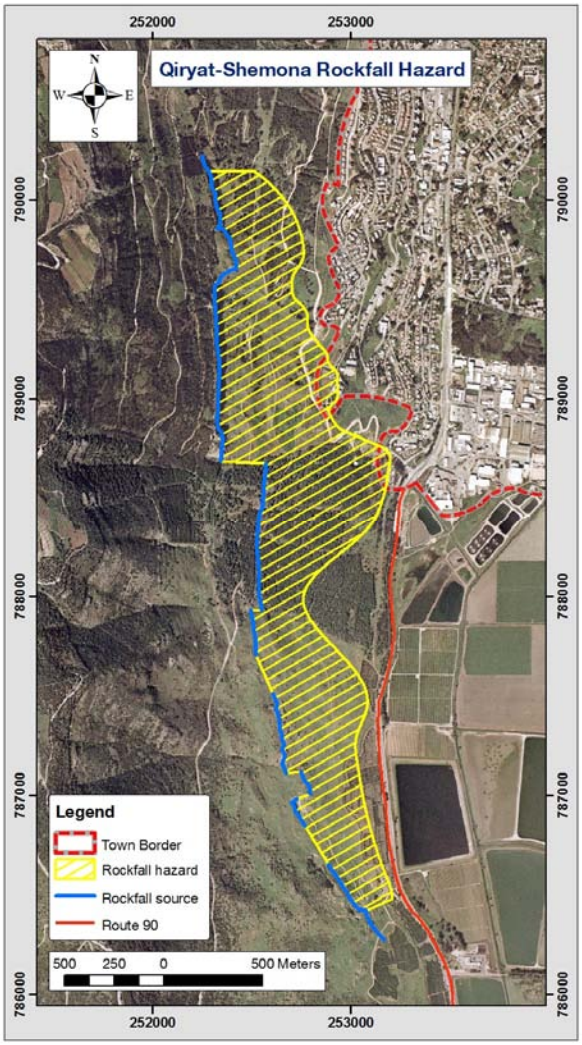

Figure 3 (top): Qiryat-Shemona OSL ages and suggested rockfall triggers. OSL age results for the past 8000 years in black circles with error bars; ages of earthquakes determined by Yagoda et al. (2008) in gray diamonds and by Kagan et al. (2007) in gray triangle; corresponding dates of earthquakes suggested as rockfall triggers in gray lines and labeled at top axis.

Figure 4 (left): Rockfall hazard map of Qiryat-Shemona. Source of rockfall (Ein-El-Assad formation) marked in blue line; area subject to rockfall hazard (from source escarpment to 100% of blocks stop line) dashed in yellow; town border line in red dashed line; Route 90 in orange solid line. Map compiled from maximal travel distance (100% of blocks stop line) of 25 simulation profiles performed using CRSP v4.

Sea of Galilee

18.2.2009

Field leader

Shmuel marco


N
1
Safed
2
Ateret Fortress
Golan Heights
Sea
of
Galilee
Tiberias
3
Susita
0
2
4
8
Kilometers

Paleoseismic study of earthquake induced landslide hazard in the city of Safed, northern Israel

Oded Katz[1]*

Geological Survey of Israel

odedk@gsi.gov.il

* Field guide

1. Introduction

The field trip focuses on the city of Safed (northern Israel, Fig, 1,which was repeatedly and severely damaged from earthquake induced landslide (EILS) which were triggered by strong-major historical earthquakes (Wachs and Levitte, 1981). The city of Safed is located on an elevated area bordering the tectonically active Dead Sea Transform (DST; Fig. 1). It was settled as early as the Roman times (1st century CE) on a narrow hill, more than 800 m above sea level ('the Citadel', now in the city's center; Fig. 2a). Katz and Crouvi (2007) found that parts of the city are built on a few meters depth of layered anthropogenic material which was deposited as a result of more than 2000 years of human habitation. The anthropogenic material is mechanically weak, susceptible to slope failure and to amplification of seismic shaking.

The field trip follows Katz and Crouvi (2007). It examines field and historical evidence for slope instability in the core city of Safed and evaluates the current EILS hazard using a GIS-based Newmark analysis (Newmark, 1965) following Jibson et al. (2000). It focuses on the significance of the anthropogenic talus/strata as the controlling factor of the slope instability in past disastrous earthquakes and its contribution to the current-hazard in Safed, as well as in similar modern populated centers that share long habitation histories.

Our Results show that earthquakes of magnitudes (MW) 5,6, and 7 at distances of up to 10km,50km and more than 100km, respectively, are likely to induce landslides in the city of Safed. The current engineering status of the city is poor and as a consequence severe damage and loss of life are expected in future earthquakes due to EILS, unless major engineering efforts are made. Comparable cities in the Eastern Mediterranean with long habitation histories (e.g., Jerusalem, Tiberias, Nablus, Amman), are expected to have similar geotechnical problems throughout their old parts. Furthermore, we think that magnitude evaluation of historical-earthquakes based on reported local-damage may yield overestimated magnitude when the damaged site is built on anthropogenic talus (a common setting in the vicinity of the Dead Sea Transform).

2. Field trip stops:

Stop 1: 'The Citadel' area; Geological setting

The bedrock under the built parts of the city consists of Upper-Cenomanian to Eocene dolomite, limestone, chalk, and marl (Fig. 2). Nevertheless, in the frame of the current study we found that most of the core city is built on talus/strata of anthropogenic material up to 10m thick that was deposited on top of the above rock sequence in the course of the long (~2000 years) habitation. The anthropogenic material is typical of an archeological mound 'tell' (Rosen, 1986) and in the studied area it exhibits two types: (1) talus-like inclined (up to 30°) layers of pebbles and pottery embedded in unconsolidated, thin earth-like material (Fig. 3a); this type is exposed mainly around the citadel, and (2) ruins of man-made stone structures filled and covered by reworked sediments (Fig. 3b).

Stop 2: The old city core; Field evidence for slope instability

Tens of sites showing evidence for past and current slope instability were mapped in the studied area (marked by arrows in Fig. 2a, b). This instability is attested in the core city limits by lamp posts based in the anthropogenic talus that are tilted (Fig 4a). Likewise, open cracks, which in some cases approach total structural failure, are common in road pavements, walls, and buildings (Fig. 4b-c). The above field evidence reveals that the anthropogenic talus exposed in the core city is statically unstable and is creeping down slope. This creep shifts the material towards its residual strength and we anticipate that under dynamic earthquake conditions landslides will develop. During the rainy winter season, meter-scale shallow slumps and debris flows are common in the anthropogenic talus (Fig. 4d).

Outside the core city area, within the new city limits, disrupted shallow slides and slumps were found in natural and cut slopes. Rock falls occur where dolomites and limestones are exposed in steep slopes.

Stop 3: Above the old cemetery; EILS hazard analysis

a. Historical evidence for EILS

Historical research indicates that parts of the core city of Safed were repeatedly, and heavily, damaged during earthquakes in the last centuries (M_S ~6.6, Oct. 1759; M_S >7.0, Jan. 1837). We believe that this damage is mainly a result of landslides, considering the steep slopes and the weak geological material the city is founded on. The historical evidence (Thomson, 1873; Ya'ari, 1943; Ben-Horin, 1952; Schiller, 2002; Yizrael, 2002a,b) constrain the limits of the area in which EILS occurred during earthquakes (Fig. 2b). We used these constraints on the areas of the EILS together

with the field evidence of slope instability to calibrate the mechanical model of the EILS hazard Newmark analysis.

b. Calibration of the model

Two historical earthquakes that induced landslides in Safed (Oct. 1759 and Jan. 1837) and one earthquake that did not (Aug. 1984, M=5.3; epicenter is shown in Fig. 1) were used for calibration of the mechanical model. By fine tuning of the mechanical model we achieved reasonable similarity (based on visual comparison) between the map of calculated dynamic slope instability in a given earthquake and the field and historical landslides map of the same earthquake (Fig. 5a, b). After calibration, we were able to simulate earthquake scenarios and analyze which of the earthquakes would cause EILS in the Safed.

c. Current EILS hazard in the city of Safed

We calculated slope performance for 24 scenario earthquakes, assumed to be possible along the central part of the DST. Calculations show that magnitude 4 earthquakes at the minimal source distance of 10km will probably not induce landslides in the studied area (Fig. 6). Magnitude 5 earthquakes will induce landslides in Safed at source distance of less than 10km. Magnitude 6 earthquakes will not induce landslides at source distances of more than 50km, but at shorter source distances EILS will be significant. A magnitude 7 earthquake will induce landslides even at distances of more than 100km.

d. Geotechnical consideration of the anthropogenic talus

As discussed above, the anthropogenic talus underlying most of the core city is a major source of EILS hazard in the studied area. This material is apparently a source of additional seismic hazard: the amplification of seismic-shaking. The anthropogenic talus is poorly consolidated and its shear wave velocity is expected to be very low with a velocity contrast with the underlying bedrock. This setting will probably result in amplified seismic shaking that will increase the likelihood of slope failure.

The anthropogenic material is a source of enhanced seismic hazard and a significant contributor to repeated damage due to earthquakes in sites with histories of long human habitation. Each destruction-rebuilding cycle makes the site more vulnerable during the next earthquake.

The nature of the anthropogenic talus may also affect the evaluation of the magnitude of historical earthquakes, if solely based on reported local-damage (e.g., MSK, Bath 1973). Since site amplification is usually not considered in such evaluations (Ambraseys et al., 1994), the assessed historical magnitude may be misleadingly high (relative to a bedrock site). This is especially true for the long record of earthquakes in ancient cities in the vicinity of the Dead Sea Transform.

3. References

Ambraseys, N. N., Melville, C. P., Adams, R. D., 1994. Macroseismic information: The seismicity of Egypt, Arabia, and the Red Sea - A historical review: Cambridge Univ. Press, Cambridge, Mass, 19–110.

Bath, M., 1973. Introduction to Seismology. Birkhauser, 395 p.

Ben-Horin, U., 1952. An official report on the earthquake of 1837. Isr. Exp. J., 2, 63-65.

Jibson, R. W., Harp, E. L., Michael, J. A., 2000. A method for producing probabilistic seismic landslide hazard maps, Eng. Geol., 58, 271-289.

Katz, O., Crouvi, O., 2007. The geotechnical effects of long human habitation (2000< years); earthquake induced landslide hazard in the city of Safed, northern Israel. Engineering Geology, doi:10.1016/j.enggeo.2007.07.008.

Keefer, D.K., 1984. Landslides caused by earthquakes. Geological Society of America Bulletin 95, 406-421.

Levitte, D., 2001. Geological map of Israel, Sheet 2-III: Safed, Geological Survey of Israel. 1 map.

Newmark, M. N., 1965. Effects of earthquakes on dams and embankments. Geotech. 15 (2), 139-160.

Rosen, A. M., 1986. Cities of clay, the geoarcheology of Tells. Prehistoric Archeology and Ecology Series, Karl W. Butzer and Leslie G. Freeman (eds.). Univ.Chicago Press Chicago and London.

Schiller, E., 2002. The 1837 earthquake in Safed. Ariel 157-158, 106-112 (in Hebrew).

Thomson, W. M., 1873. The land and the book. Nelson and Sons, London.

Wachs, D., Levitte, D., 1981. Earthquake induced landslides in the Galilee. Isr. J. Earth Sci., 30, 39-43.

Ya'ari, A., 1943. Letter written by the Jews in Israel to their brothers in the Diaspora from Babylonian Exile to nowadays Zion Return. Gazit, Tel-Aviv, 357-367 (in Hebrew).

Yizrael, R., 2002a. The chronicles of the Jewish quarter in Safed. Ariel 157-158, 203-215 (in Hebrew).

Yizrael, R., 2002b. The old Jewish cemetery in Safed. Ariel 157-158, 216-225 (in Hebrew).

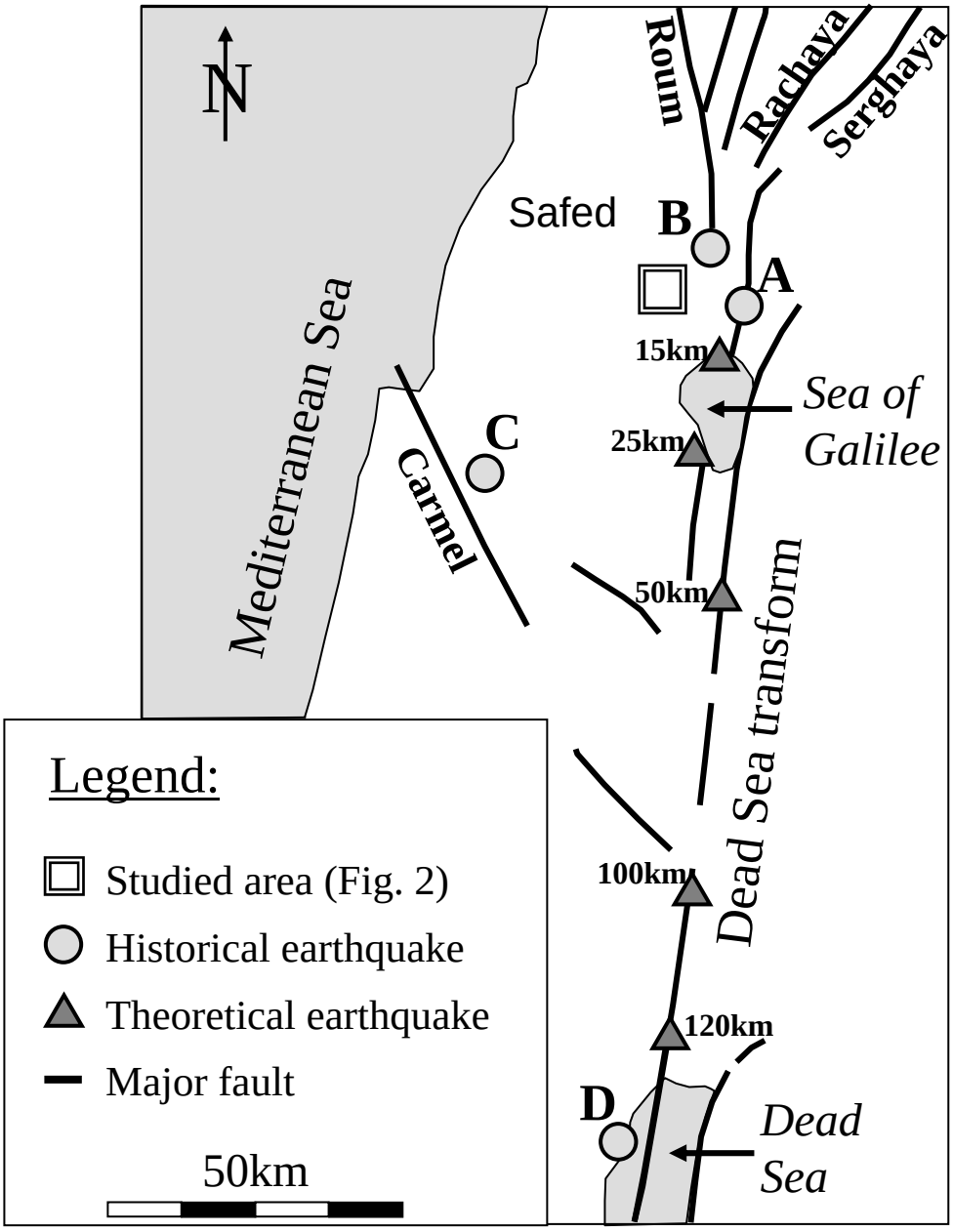

Figure 1: Major fault lines of Dead Sea Rift in the vicinity of Israel. Inferred epicenters of historical earthquakes are marked by gray circles. A is MW = 6, 1759 earthquake; B is MW = 7, 1837 earthquake; C is MW = 5.3, 1984 earthquake; D is MW = 6.5, 1927 earthquake; for details and references see text). Epicenters of scenario earthquakes are marked by gray triangles with distances from the core city of Safed) and are used to analyze EILS hazard in the studied area which is marked by double-line rectangular and shown in detail in Fig. 2.

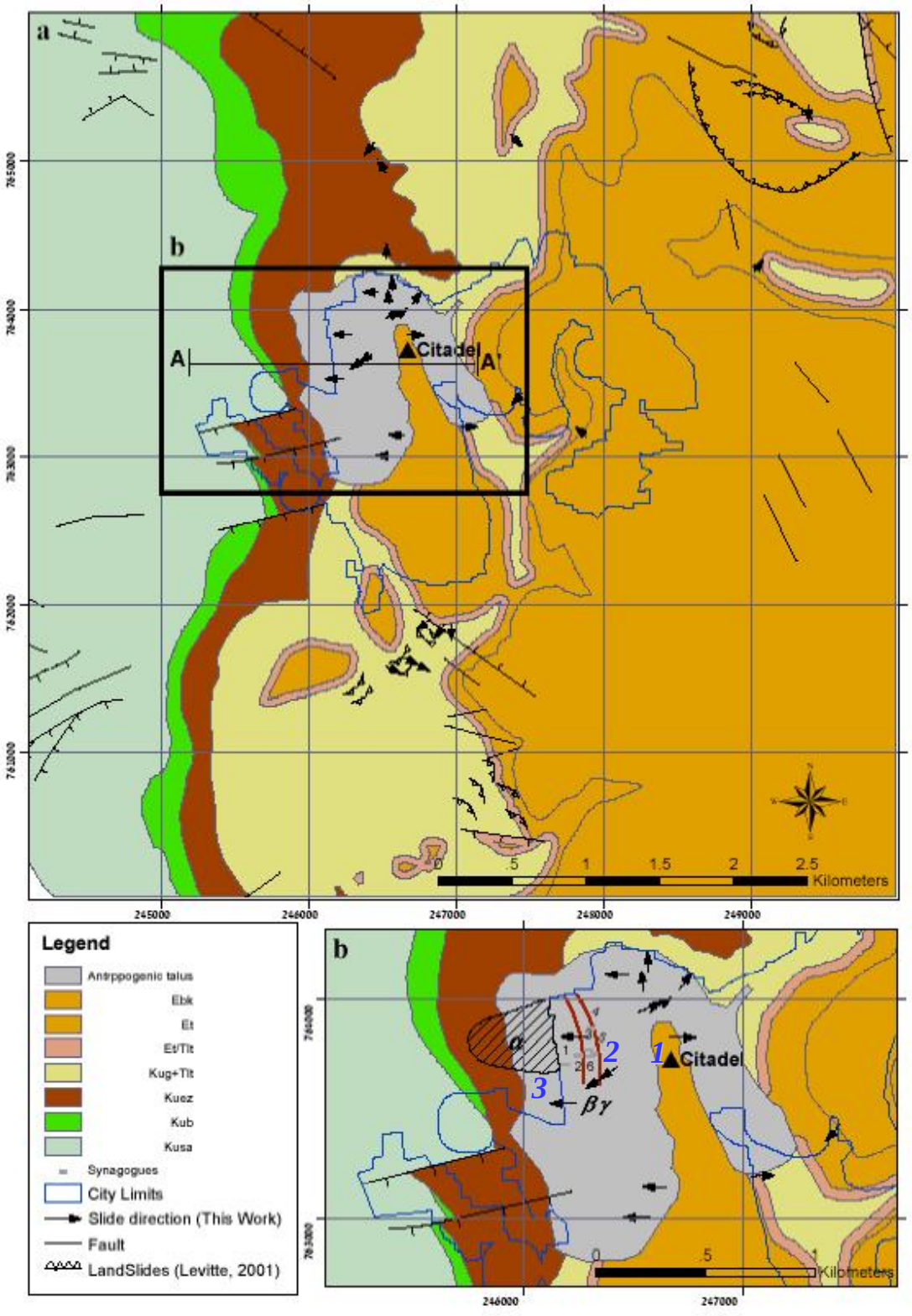

Figure 2: (a) geological map of the studied area (Levitte, 2001; anthropogenic material mapped in Katz and Crouvi, 2007). The current Safed city limits are marked by a blue solid line; (b) the core (historical) city area. The core city extended from the Citadel, westwards to the old cemetery (a). Sites of field-observed slope instability are marked by black arrows. Also shown are upslope limits of EILS area in the 1759 and 1837 earthquakes (b and g, respectively) according to reported damage to synagogues (marked by close squares where 1 is Sefaradic Ari, 2 is Banea, 3 is Hagadol/Abuhav, 4 is Greek pilgrimages/Ashkenazic Ari, 5 is Karo, 6 is Elshiech). Stops of the field trip are marked by italic blue numbers.

Figure 3: Types of anthropogenic material typical of an archeological mound ('tell') outcrop in the core city of Safed: (a) talus-like, inclined (up to 30º) layers of pebbles and pottery embedded in unconsolidated earth-like thin material and (b) ruins of man-made stone structures filled and covered by reworked thin sediments. The current city (shown in the upper part of the picture) is built on top of the ruined structures.

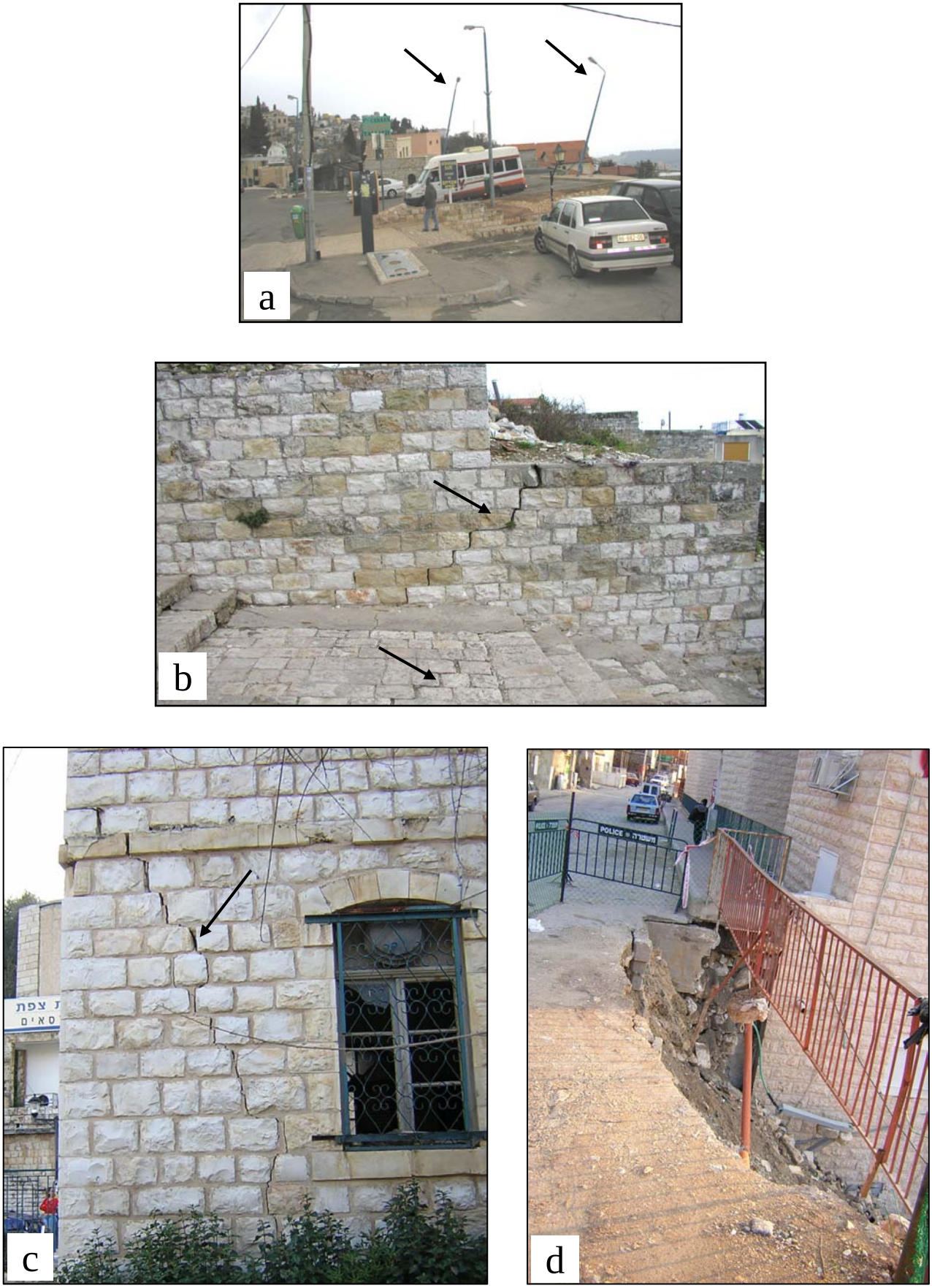

Figure 4: Field evidence for instability of the anthropogenic material slopes.
(a) inclined lamp posts found in the anthropogenic talus (marked by arrows); (b) open cracks (marked by arrows) in retaining wall and (c) in building, both found in the anthropogenic talus; (d) rainy winter-season slump in the anthropogenic talus.

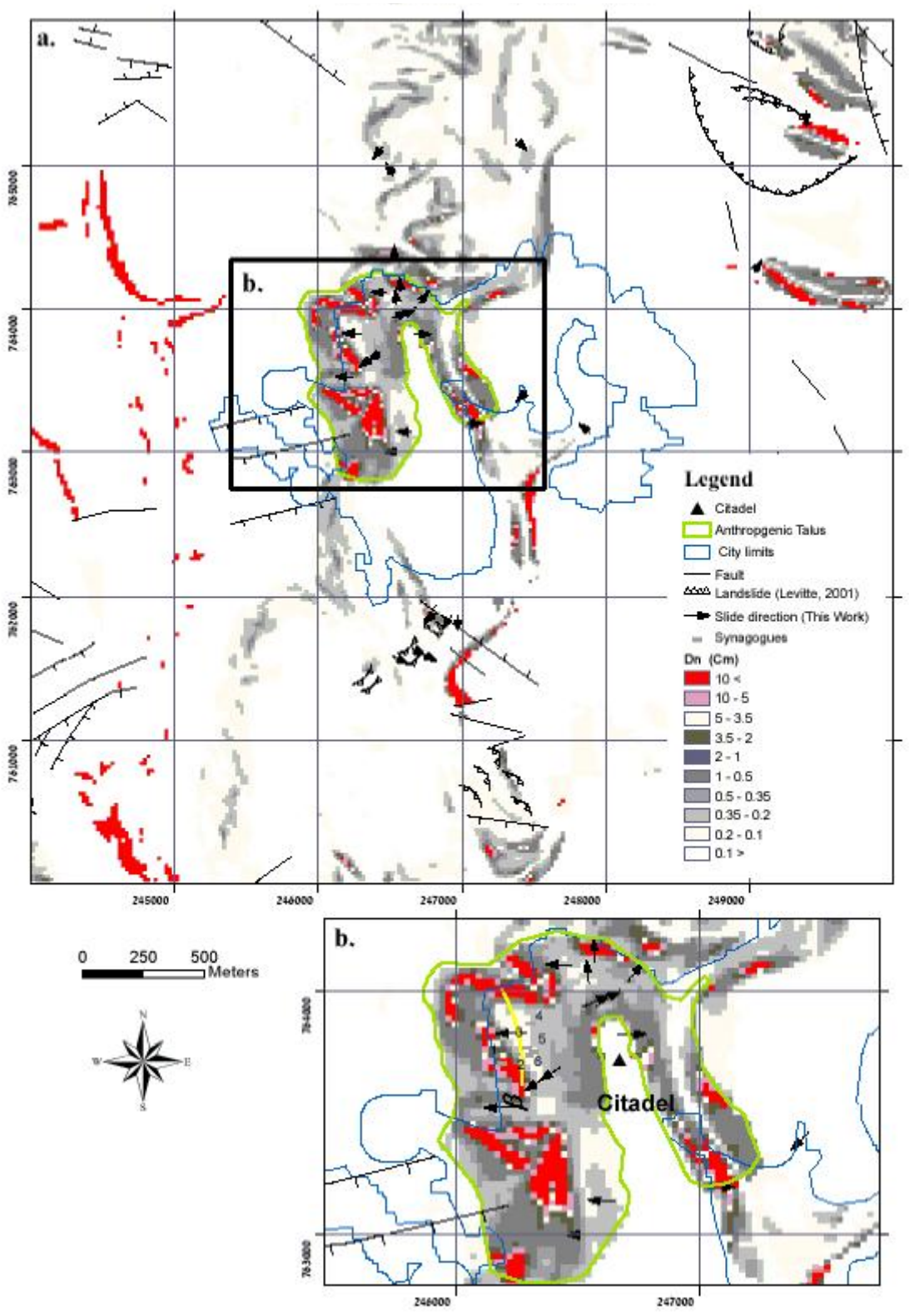

Figure 5: Calculated Newmark displacement maps of two historical earthquakes used to calibrate the mechanical model, (a-b) October 1759 MW=6, R=15 earthquake; (c-d) January 1837 MW=7, R=10 earthquake. For inferred location of epicenter see text and Fig. 1. Also shown are upslope limits of EILS area in the 1759 and 1837 earthquakes (b and g, respectively, see Fig. 2) traced according to reported damage to synagogues (marked by numbered close squares, see Fig. 2).

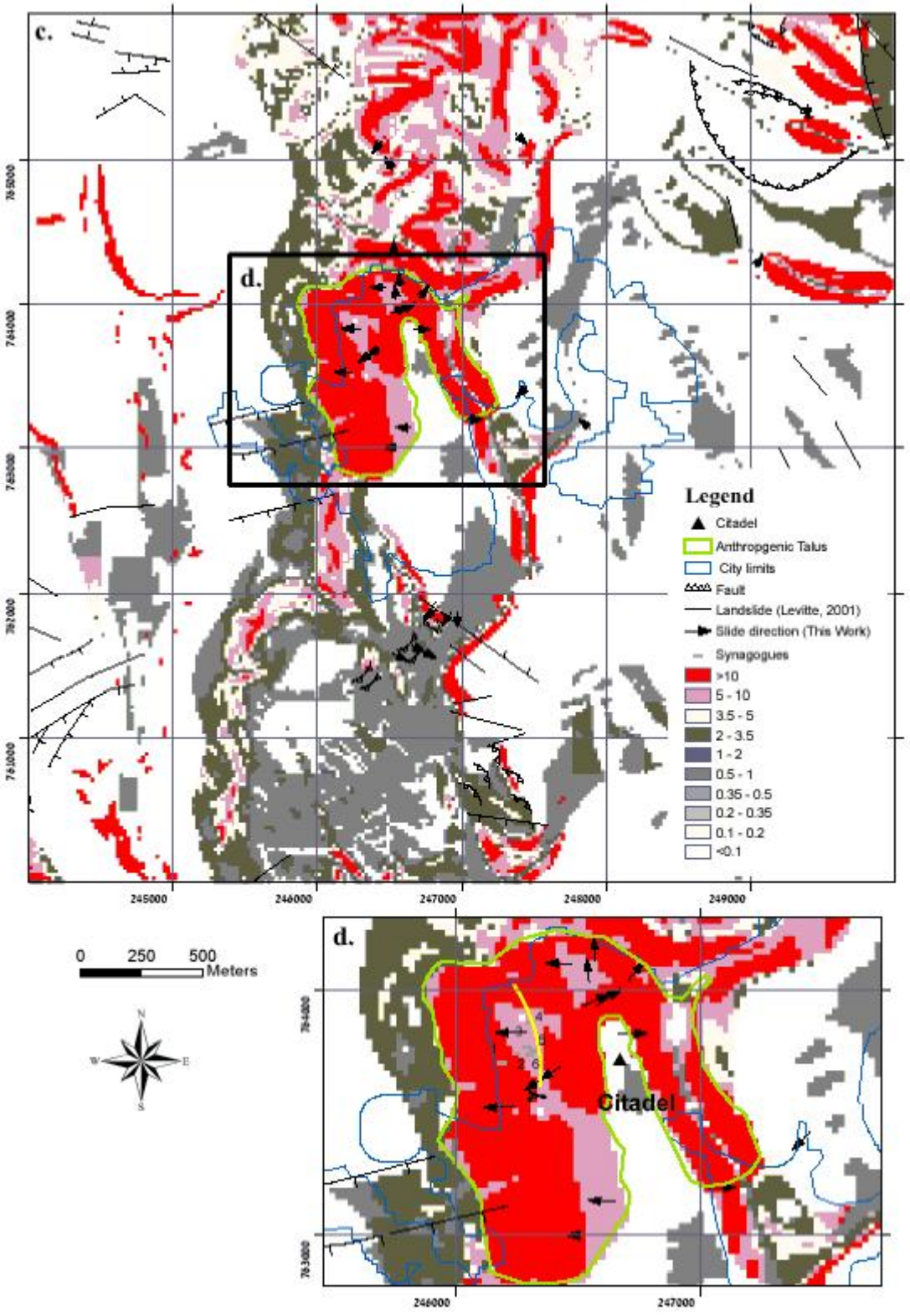

Figure 5: Continue.

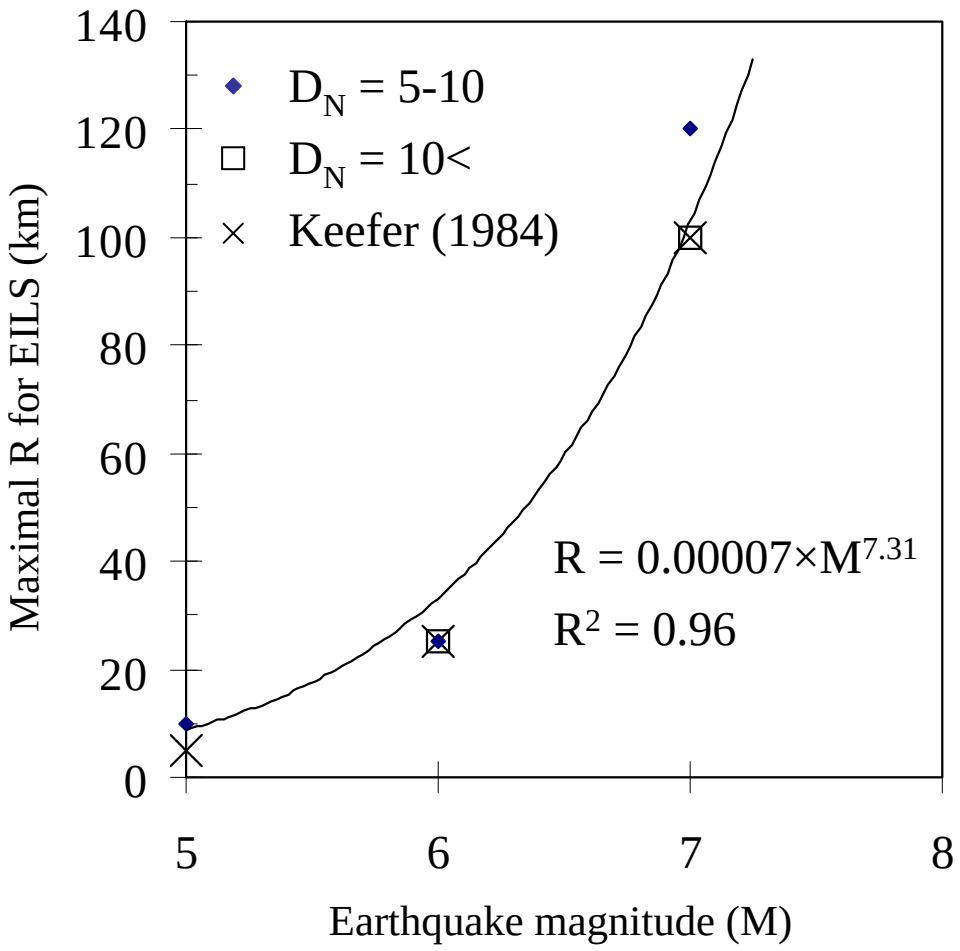

Figure 6: Maximum fault zone distance (R, km) for EILS (threshold DN values are 5-10cm or >10cm, for the conservative cases, respectively) as a function of the triggering earthquake magnitude (MW). Data is from the calculated scenario earthquakes (for location see Fig. 1). Also plotted are the maximum fault zone distances for EILS according to Keefer (1984).

The history of the Frankish Castle of Vadum Iacob

Shmuel Marco[1]*

[1]The Department of Geophysics and Planetary Sciences, Tel Aviv University

shmulikm@tau.ac.il

* Field guide

Source: Ellenblum, R., 1998, Frankish Rural Settlement in the Latin Kingdom of Jerusalem: Cambridge, England, Cambridge University Press, 321 p.

The Frankish Castle of Vadum Iacob [meaning :"Jacobs' ford"], was known also in the 12th century by its Arabic name: Bayt al-Ahzan, [meaning "The House of Grief"] or by its 13th century name of Le Chastelez. Today it is known by the Hebrew name Metzad ‘Ateret [castle of abundance] which is derived from the modern Arabic name Qasr al-‘Atara.

Vadum Jacob dominated the only crossing of the Jordan River south of the Hulah swamps and north of the deep Jordan canyon. The site is a day’s walk from Damascus and half day, according to Al-Muqadasi, from Tiberias or Safad.

The castle was built above the west banks of the River Jordan in the place commonly called “Jacob’s ford”. According to the 13th century Frankish chronicler Ernoul, the place was in the Muslim and not in Frankish territory. The Franks built their castle because they wanted to weaken the most vulnerable part of the Muslim’s frontier

The other possible crossing from Syria to Palestine north of the Sea of Galilee was near the city of Banyas, which was held by the Muslims. It is also possible that Vadum Iacob was even planned to threaten the Muslim center of Damascus.

The King (which king?) made a general call to arms, gathered the whole army in Vadum Iacob and stayed there from the beginning of October, 1178 until the second week of April, 1179. The beginning of the works in October might be attributed to climatic considerations as the heat in the upper Jordan Valley from June to the end of September is unbearable. The temperatures decrease considerably in October. The rainy seasons also starts by the end of October and the rains reach their peak in December, January and February. This schedule left the builders with two months of intensive work in mild weather before the beginning of the rainy season.

William of Tyre stresses that the construction of the castle was already completed when the king left for Jerusalem in the beginning of April, 1179. In other words, he claims that the monumental castle was finished after only six months of work. William was not an eye-witness, since he had left the country several months earlier on his way to Rome, but he also writes that in

mid-April 1179, following a battle between Franks and Muslims near Banyas, the Franks carried the dying Constable, Humphrey of Turon, "to the new castle which was still under construction." This statement was interpreted as proof that the castle was not finished when the king left for Jerusalem.

Our excavations reveal that the construction of the castle was not completed at the time of its destruction in August, 1179. Remains of construction works were excavated throughout the castle. We unearthed a complete inventory of medieval working tools: spades, hoes, picks, a wheelbarrow, plastering spoon, scissors, etc. A dramatic find adjacent to one of the gates was a heap of lime with working tools imbedded in it, which was covered by Muslim arrowheads. That clearly demonstrates how the builders where interrupted by the sudden attack.

A similar discrepancy is found in the description of the construction of the castle of Safad, which was built between 1240 and 1260. Benoit, the Bishop of Marseille wrote that when he left the site, after less than six months of work, the castle was already finished, and was in a defensible state. However, when he himself returned there 20 years later, he was impressed by the outer wall, which was added to the castle since his first visit. He himself does not explain how a castle can be "finished and in a defensible state" while the outer wall was only added later.

We can assume that the construction of the inner curtain wall was completed by then, and the four hot months of summer were devoted to improving the conditions of life inside the castle and to preparing for an intensive building season, planned, without doubt, for the cool autumn and winter months.

According to Ibn Abi Tayy, [as quoted by Abu Shama] Salah al-Din tried to buy the castle from the knights Templars and negotiated possible terms. The Franks, so it seems, were willing to consider the destruction of the castle if the Muslims paid the estimated cost of its construction. The Sultan offered 60,000 dinars and was even willing to offer 100,000 dinars because "the Templars provided it generously with garrison, provision and arms of all kinds". Salah al-Din promised his men to destroy the castle by himself, once it was taken.

It seems that Salah al-Din was reluctant to challenge the entire Frankish army and dared to attack only when the army was no longer present. He visited the site immediately after the departure of the king in April 1179, accompanied by a representative of the Khalif, Qadi al-Fad'il. He probably considered the advance of the works, weighing the possibilities of taking it by force, or buying it. Immediately after the failure of the negotiations, in May 16th 1179, Salah al-Din attacked the site for the first time. He stayed there for five days and failed to take it by surprise.

The decisive attack on the castle commenced on Saturday, 19th Awal, 575\August 24th 1179, the Muslim forces being commanded by Salah al-Din himself and his best generals. Salah al-Din realized that it will be difficult to take the castle by assault and opted for digging under the walls. The result of the first attempts was very poor. The tunnel was 30 feet in depth and 3 feet in width, whereas the width of the wall was 12 feet. The timber that supported the tunnel was set

on fire but the wall did not collapse. Salah al-Din was in a hurry; he could not wait for the fire to be extinguished gradually. He therefore promised a dinar for every skin full of water, which will be poured onto the flames.

When the fire was extinguished and the sappers dug to a deeper and wider tunnel, which they set on fire once again on Wednesday. Finally, on sunrise, Rabi' I 575 [=29 August 1179], the Muslim sappers succeeded in breaking through the walls which collapsed to the applause of the Muslims. The Franks erected a temporary timber wall, but strong wind strengthened the flames and the tents, timber and many of the Frankish warriors caught fire. The Muslim sources describe in amazement how the commander of castle jumped into the flames. The rest of the Franks asked for surrender terms.

The Muslim armies entered the castle killing many of the Frankish marksmen and taking many captives. Saladin took the armors of about 1000 knights and sergeants, 100,000 weapons and many animals as booty. The captives were led to Damascus.

The Muslim soldiers then destroyed the castle and threw the corpses of the defenders into a deep cistern. This last careless operation was probably the cause of a plague, which started within 3 days of the conquest. Saladin and his men left the site on their way to Damascus. The Frankish army in Tiberias saw their fortress caught ablaze and covered with deep smoke.

The Earthquake ruptures

The Crusader castle of Vadum Iacob (Fig. 1) was deformed by destructive earthquakes triggered by motion along the Dead Sea Transform. This is evident in the 2.1 m offset of the E-W-striking walls on the south and on the north. The first time was an M>7 earthquake at the dawn of 20 May 1202. It offset the castle walls by 1.6 m. The earthquake of 25 October 1759 accounts for the remaining 0.5 m out of a total 2.1 m of offset (Ellenblum et al., 1998).

In the last phase of excavations in Vadum Iacob we unearthed parts of a large Hellenistic compound, which we identify as a fortified settlement, built on the same strategic point on the main road between the Galilee and Syria. The Hellenistic structures complete a 23-century long record of slip. Abundant ceramics and C14 ages confirm the identification of Hellenistic buildings in the northern part of the Crusader fortress, north of the mosque and south of the southern Crusader wall outside the fortress. In both locations the Hellenistic walls are truncated by the fault. The correlation between the walls on the west and on the east is clear only in the south, where a 5.7-m-offset is inferred (Fig. 2). Crosscutting Hellenistic walls of different styles and different offsets may be explained by an earthquake in the end of the second century BCE, after which the site was rebuilt. Some supporting evidence is found in nearby archaeological sites and in a rather vague written record about an earthquake in 198 BCE (Guidoboni et al., 1994). Unfortunately there are no structures between the Hellenistic and the Crusader periods, apparently the site was abandoned. The 3.6 m displacement in this period may have been associated with one or more earthquakes.

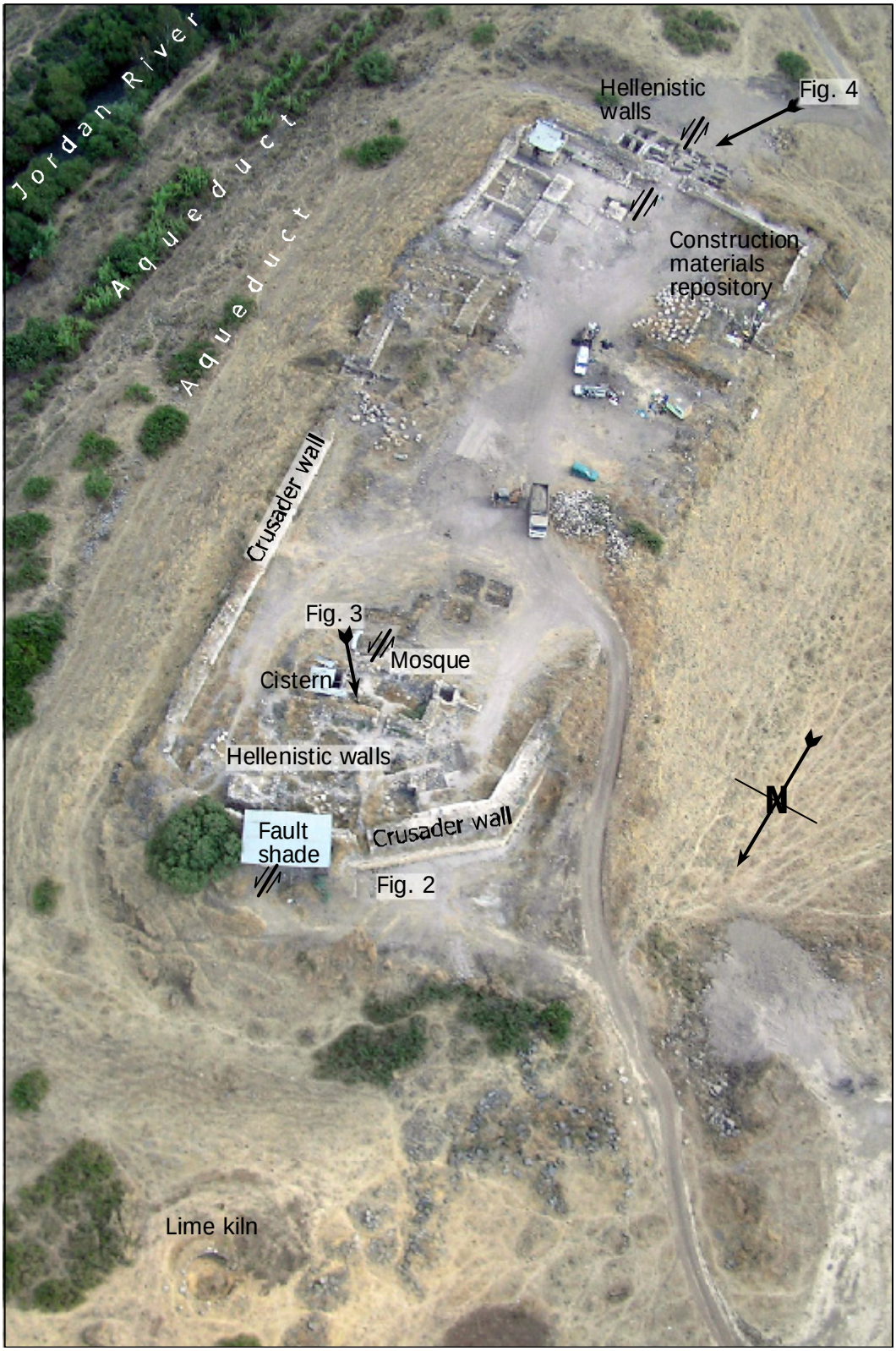

Figure 1: Oblique airphoto of the Vadum Iacob (Ateret) fortress.

Figure 2: Northern Crusader defense wall built of meticulously hewn ashlars from a quary on the hill to the west. On the left side is the construction ramp, which was used for hauling the blocks up to the high levels of the wall. The wall was actually buried as its construction advanced.

Figure 3: Faulted wall of the Ottoman mosque. Picture taken in 1994, before the excavation.

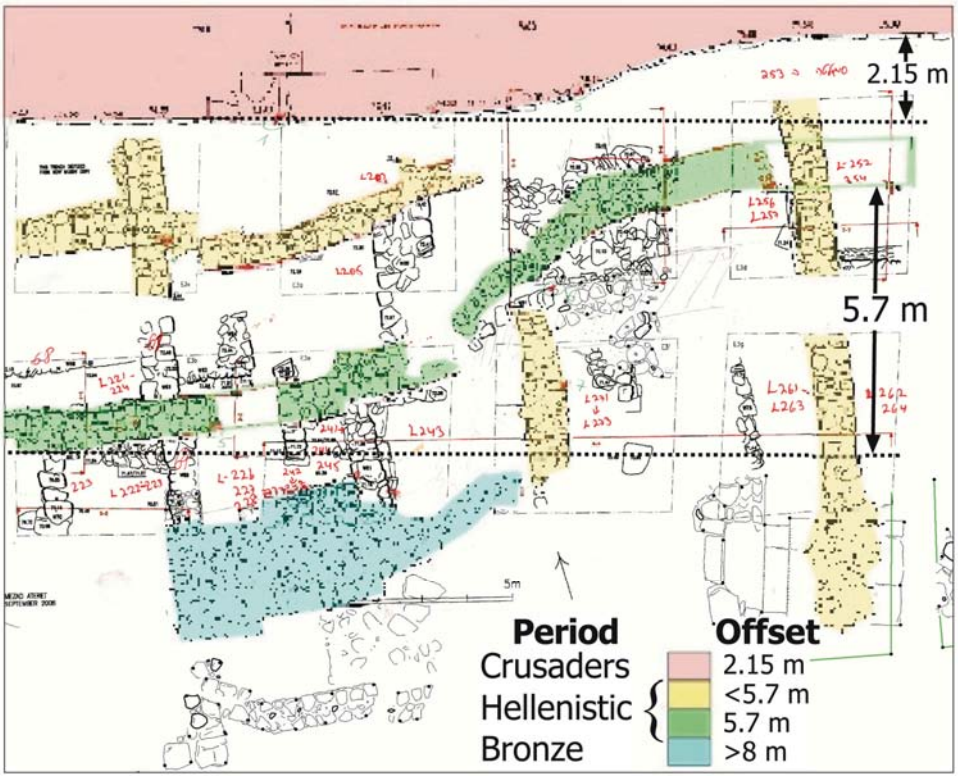

Figure 4: Two different styles of Hellenistic walls are found south of the Crusader fortress. The older walls (green) are about 60-80 cm thick, made of local basalt and limestone cobbles without cement. Their foundations are found at shallow depth of up to 1 m below the modern surface. Some of them are damaged, with the upper parts collapsed, and fallen stones are lying on the floor near them, burying whole ceramic artifacts. The artifacts are identified as 3rd century BC candles, jars, and cooking pots. The E-W trending Hellenistic walls are sheared and offset left-laterally. The location of the fault is 2-3 m west of where the Crusader wall is faulted. The second type of Hellenistic walls is made of the same materials but the cobbles are cemented, their foundations are over 1.5-2 m below the modern surface, and their width is 50 cm. They are associated with artifacts from the late 2nd and early 1st century BC. The present stage exposed primarily N-S-trending walls of this kind, which truncate the former E-W-trending walls. The fault-parallel trend of these walls does not provide any measurable for slip.

The types and the arrangement of the walls are interpreted as two construction periods separated by a destruction event, most probably associated with the left-lateral displacement of the older walls. We therefore attribute the termination of the older phase to an earthquake that occurred after the 3rd century BC and before the late 2nd century BC.

References

Ellenblum, R., 1998, Frankish Rural Settlement in the Latin Kingdom of Jerusalem: Cambridge, England, Cambridge University Press, 321 pp.

Ellenblum, R., Marco, S., Agnon, A., Rockwell, T., and Boas, A., 1998, Crusader castle torn apart by earthquake at dawn, 20 May 1202: Geology, v. 26, p. 303-306.

Guidoboni, E., Comastri, A., and Traina, G., 1994, Catalogue of Ancient Earthquakes in the Mediterranean Area up to the 10th Century: Bologna, Istituto Nazionale di Geofisica, 504 p.

Paleo PGA estimates around the Sea of Galilee from back analysis of old landslides and structural failures in historic monuments

Gony Yagoda-Biran [1*], Yossef H. Hatzor[1], Rivka Amit[2*] and Oded Katz[2*]

[1] Dept. of Geological and Environmental Sciences, Ben-Gurion University
[2] Geological Survey of Israel

yagoda@bgu.ac.il

*field guide

1. Motivation and Rationale

The estimated peak ground acceleration (PGA) for a specific region can not always be determined reliably from compilation and statistical analyses of instrumental data acquired in specific regions, because of the relatively short time window available for such an approach, typically up to 100 years of instrumentation .

In this project, we estimate paleo-PGA values on the eastern and western margins of the Sea of Galilee (Lake Kineret) using two different approaches: 1) Backward limit equilibrium analyses of ancient, seismically induced, slumps in natural rock slopes, and 2) Backward dynamic analysis of seismically driven toppling of columns at the south-eastern church of Susita, believed to have been destroyed by an earthquake dated to 749 AD. We believe that Paleo-PGA values thus obtained may constrain modern PGA estimates for the region that are based on the instrumental record only.

2. Research Methods and Preliminary Results

2.1 Backward limit equilibrium analyses of ancient landslides

Two ancient landslides are analyzed: 1) The *Ein Gev* landslide – located on the eastern margins of the Kineret, 2) The *Fishing Dock* landslide – located on the western margins of the lake.

Both slides are back-analyzed using the Morgenstern-Price Method of Slices, using the commercial software package SLOPE/W 2004. The geometry of the slope profile, ground water table level, material properties, and assumed location and geometry of the failure surface are used as input for the code. The geometry of the slope is defined using a 1:50,000 topographical map. The ground water table level is estimated on the basis of field observations. The material properties for the rock mass are determined using laboratory tests. For the Ein Gev landslide we performed direct shear tests at the rock mechanics laboratory in Ben-Gurion University. For the Fishing Dock landslide material properties are selected from data reported by Dr. Uzi Saltzman. The exact location and geometry of the sliding surfaces are assumed on the basis of field observations and borehole data.

2.1.1 The Ein Gev landslide – preliminary results

Geometrical comparison between the slumped and intact slope profiles

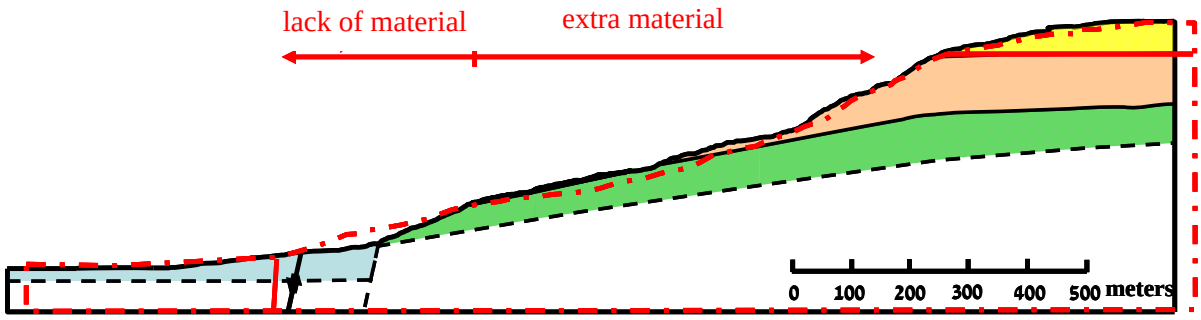

Geological section of the southern, intact, slope (colored). The profile of the slumped slope is superimposed (red dashed line). The geometrical comparison reveals lack of material in the middle section of the slumped slope, and extra material in the lower section of the slumped slope, as would be expected in a typical slump configuration.

The modeled profile of the landslide for backward analysis with Slope/W

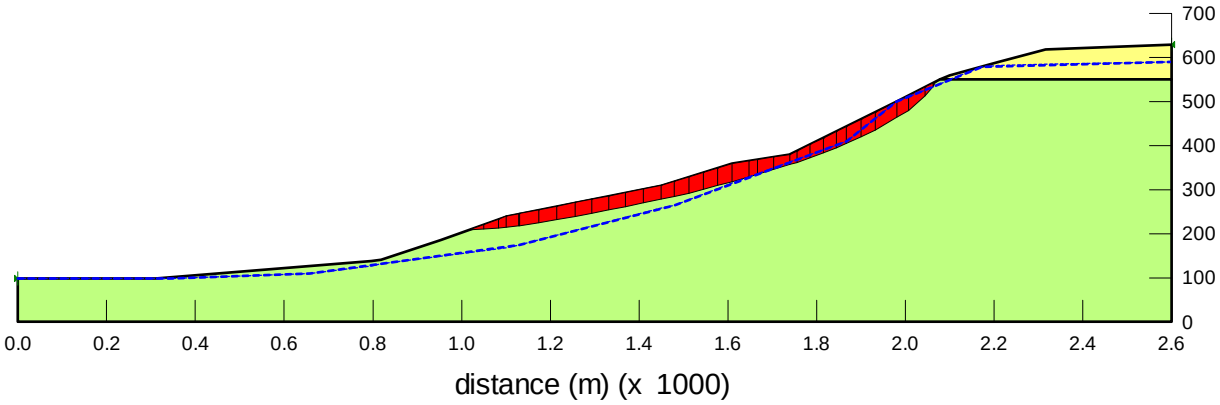

Modeled landslide profile in Slope/W. Legend: Green region - defined by the experimentally obtained material properties for the Ein Gev sands formation (= 43°, c = 370 KPa), Yellow region - undisturbed Cover Basalt formation, Red - the modeled slump, Dashed blue line - assumed ground water table level.

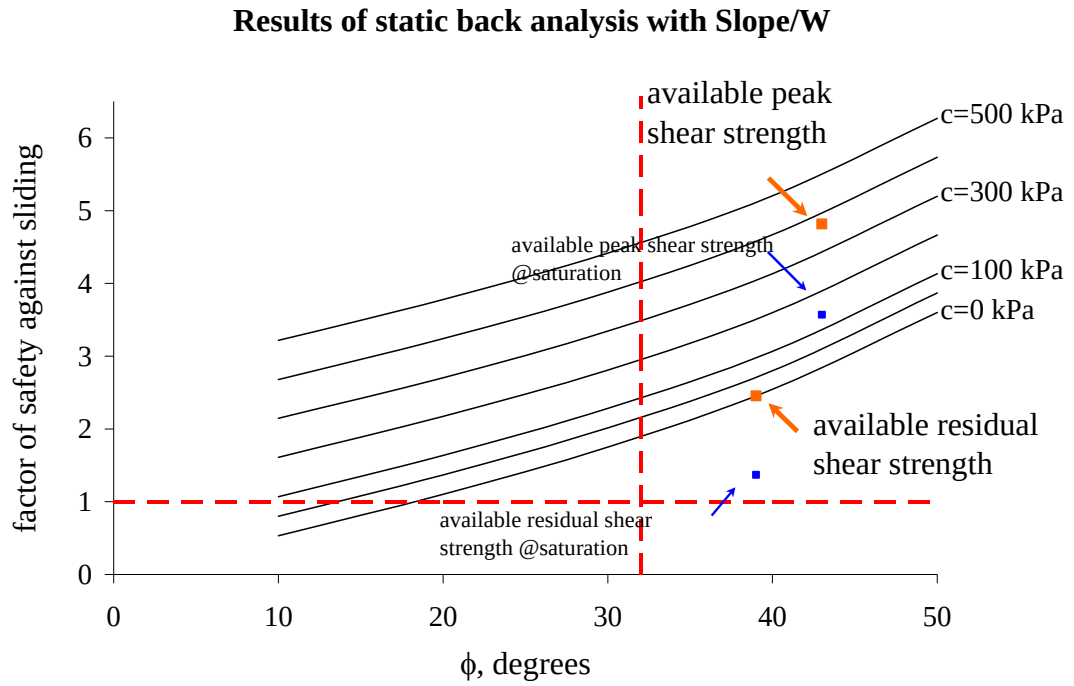

Factor of safety for static loading conditions as a function of cohesion (c) and friction angle ( ).Most results are well above the F. S. = 1 line, implying a stable slope under static loads.

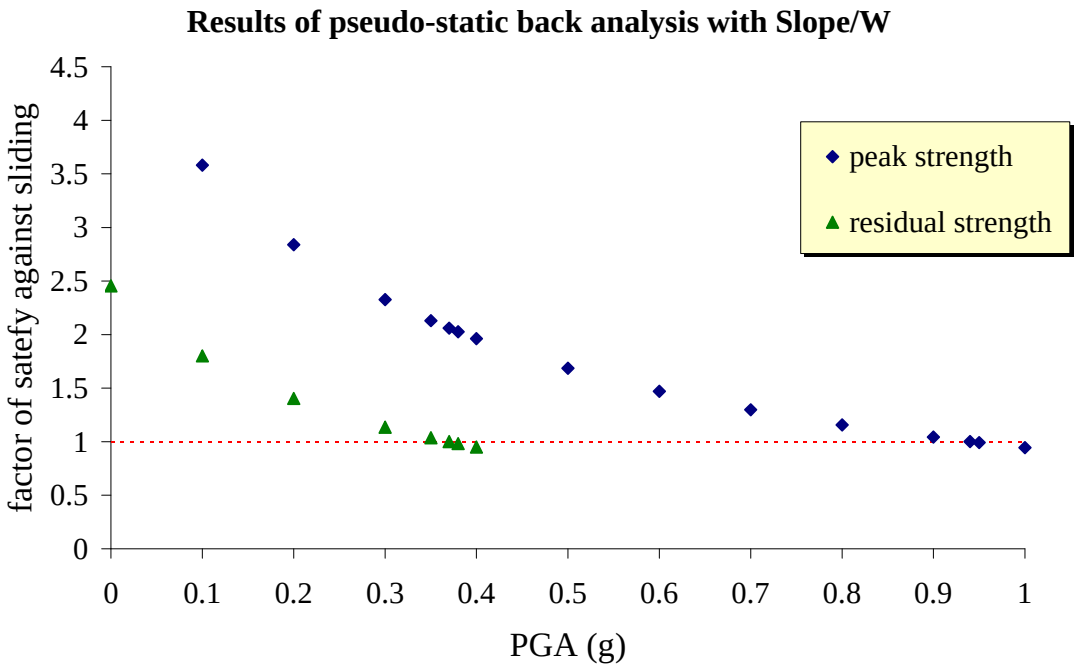

Factor of safety vs. pseudo-static horizontal force expressed in terms of horizontal PGA. The shear strength parameters are = 43°, c = 370 kPa for peak strength, and = 38°, c = 0 for residual strength. Note that with the available peak shear strength slope failure requires a PGA of 0.95 *g*. With residual strength slope failure is obtained with PGA = 0.37 *g*.

Results of a seismic reflection survey

A

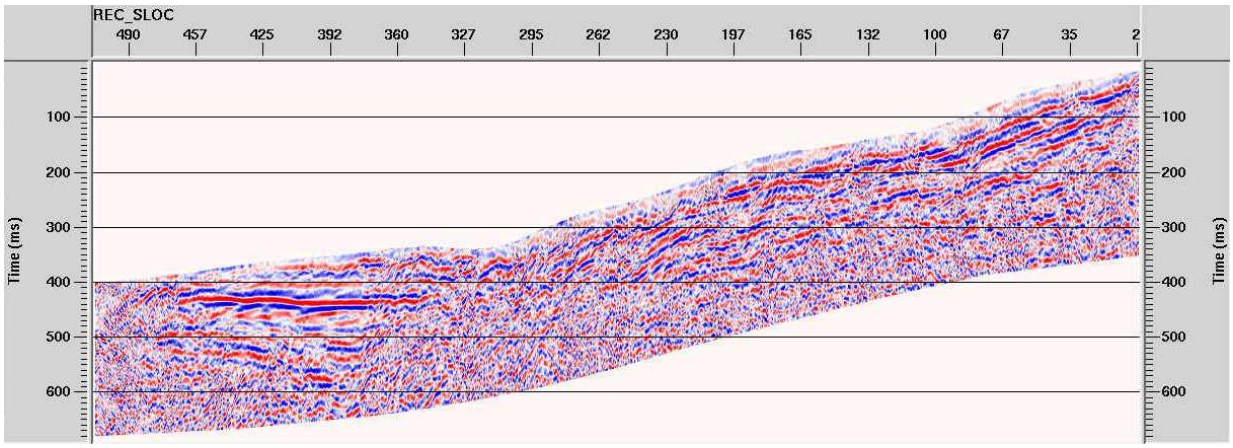

B

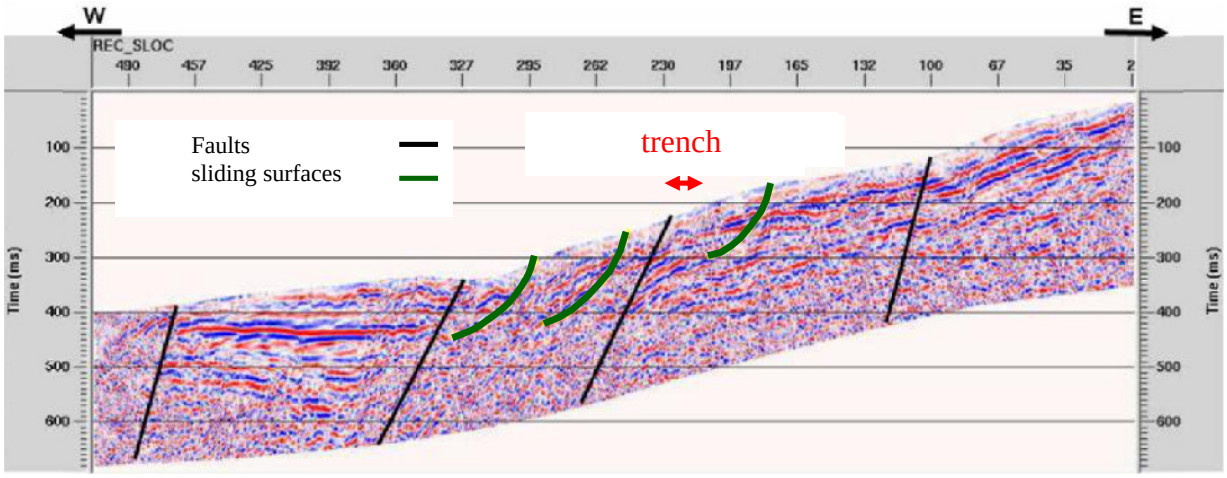

Seismic reflection survey of the slump: A) Un interpreted cross section, B) Interpreted cross section. Black lines - delineate discontinuities interpreted as faults, Green lines – delineate discontinuities interpreted as possible sliding surfaces.

2.1.2 The Fishing Dock Landslide – preliminary results

Material properties used for back analysis (Data from U. Saltzman)

Test date	Drill #	Test type (*)	Depth (m)	Lithology (**)	Cohesion (KPa)		Friction angle		Comments	Average
June, 1995	1	CD-DS	15	CH	400		46		Natural conditions	c=400 ϕ=46
Jan, 1999	1	CD-DS	24	CH	45		21		Saturated conditions	c=35 ϕ=42
Jan, 1999	2	CD-DS	16	CH	10		36		Saturated conditions	
2003	1	CD-DS	8-9	CH	0		65		Saturated conditions	
2003	1	CD-DS	11-12	CH-CL	100		47		Saturated conditions	
2003	7	CD-DS	14	CH	20		42		Saturated conditions	
					Total	effective	Total	effective		
May, 1996	1	CU-TX	15	CL	400	350	16	23	Saturated conditions	c_T=86 ϕ_T=33
May, 1996	1	CU-TX	19	CL	50	0	44	48	Saturated conditions	
May, 1996	3	CU-TX	20	MH	20	36	10	46	Saturated conditions	
Jan, 1998	3	CU-TX	5	MH	25	5	32	36	Saturated conditions	
Jan, 1998	3	CU-TX	3	CH	25	10	39 (res)	33 (res)	Saturated conditions	
2003	2	CU-TX	12	CH	0	10	24	31	Saturated conditions	

Modeled profile of the Fishing Dock landslide for backward analysis with Slope/W

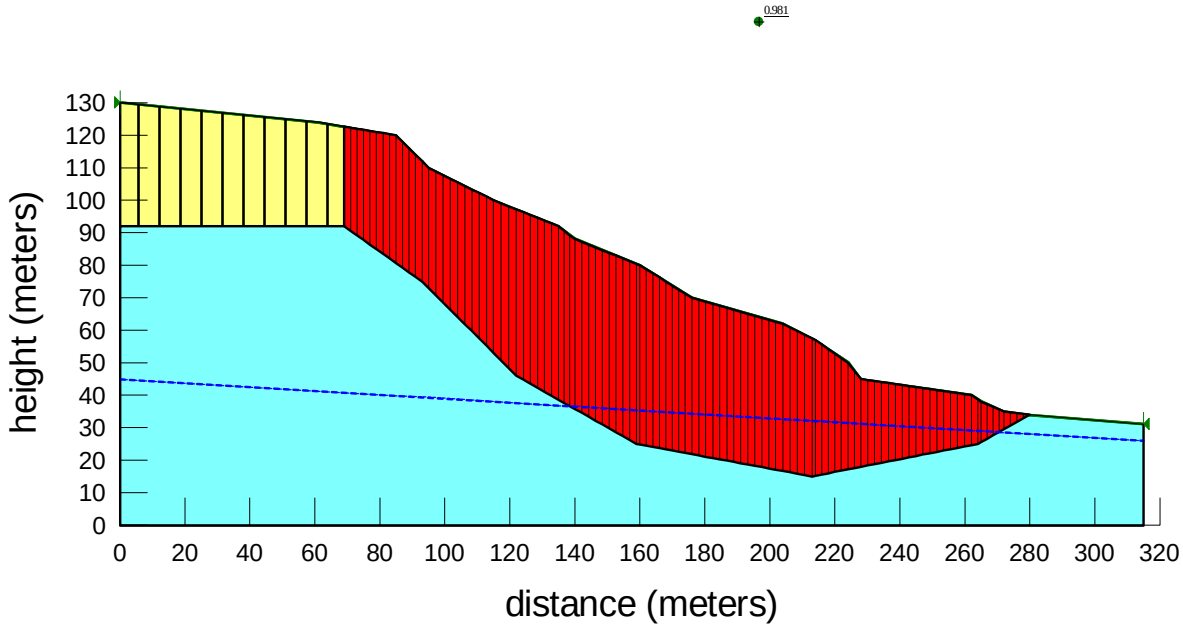

The modeled profile in Slope/W. Legend: Blue - material properties compiled from Saltzman's data, Yellow – Cover Basalt, Red – slump, Dashed blue line – assumed GWT.

Concentrated limit equilibrium analysis results - the Fishing Dock landslide

Run #	Ground water table	Material strenth	Static Factor of Safety	Pseudo-Static PGA (g)
1	recent	Natural, drained	4.9	1.61<
2	recent	Saturated, drained	2.8	0.85
3	at surface	Saturated, drained	1.52	0.28
4	recent	Saturated, undrained, total	2.3	0.5
5	at surface	Saturated, undrained, total	1.35	0.15

2.2 Backward dynamic analysis of the toppled columns at Susita with the numerical DDA method

The dynamic analysis was performed using the DDA (Discontinuous Deformation Analysis) method - an implicit discrete element method. DDA models a discontinuous material as a system of individually deformable blocks that move independently with minimal amount of interpenetration. The formulation is based on dynamic equilibrium that considers the kinematics of individual blocks as well as friction along the block interfaces.
The DDA needs as input the geometry of the column and its physical properties (density, friction angle, Young's modulus), as well as some numerical parameters.

2.2.1 The modeled cathedral column at Susita – preliminary results

The modeled column in DDA

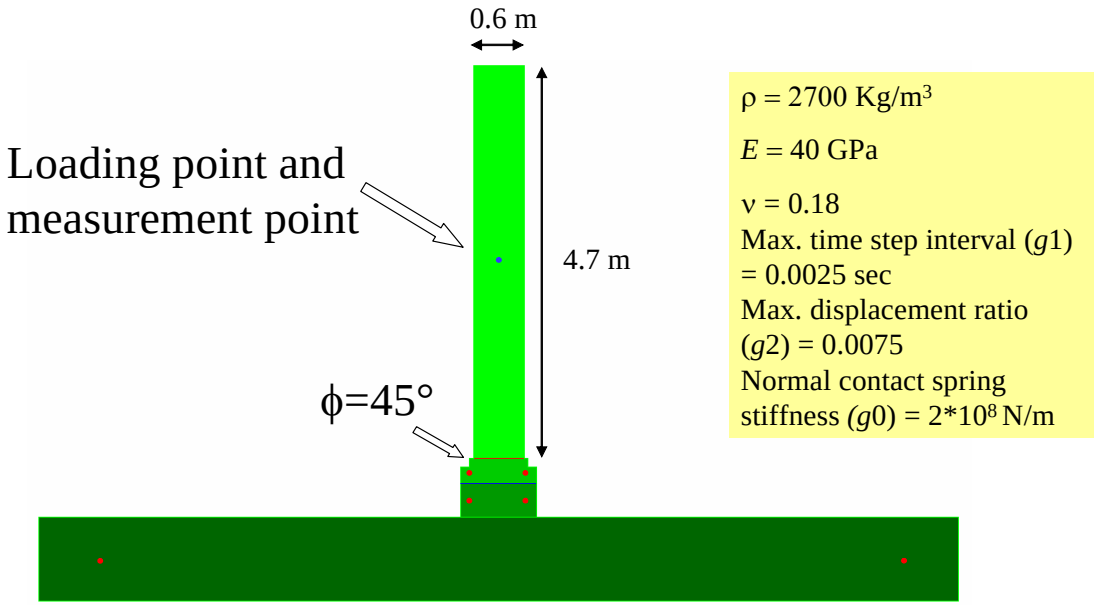

Concentrated results for DDA simulations with different earthquakes as input

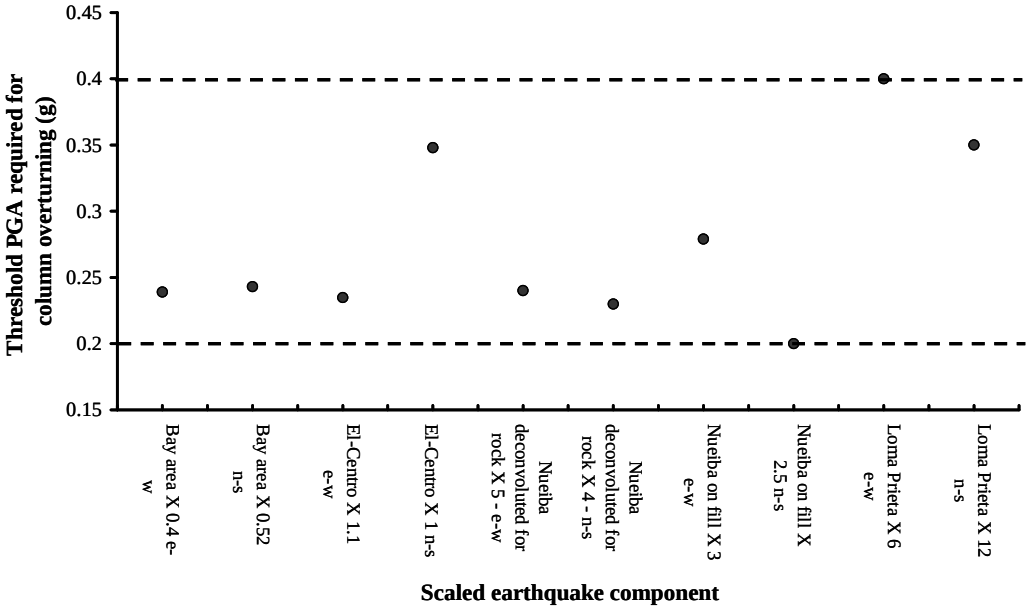

Threshold PGA values required to topple the modeled column with DDA, using different earthquake records as input acceleration. Five different earthquakes are used: the Nuieba 1995 as recorded in Eilat, the Nueiba 1995 record deconvoluted for rock response, a San Francisco Bay area design earthquake (synthetic), the Loma Prieta 1989 record measured on rock, and the Imperial Valley 1940 record measured on fill. Each record is used twice: 1) N-S + vertical component, and 2) E-W + vertical component, resulting in 10 records. The records were either up-scaled or down-scaled to obtain the threshold PGA required for toppling. Note that although the records are from different fault systems, measured on different subsurface conditions, and have different frequency contents, the obtained range of threshold PGA values required for column toppling is rather narrow: between 0.2 and 0.4 *g*.

Paleoseismology of the Eastern Sea of Galilee

Rivka Amit[1*], Oded Katz[1*], Gony Yagoda-Biran[2,1*], Yossef H. Hatzor[2]

[1]Geological Survey of Israel
[2]Dept. of Geological and Environmental Sciences, Ben-Gurion University

rivka@gsi.gov.il

* Field guide

The study site is located between the western slopes of the Golan Heights and the eastern coast of the Sea of Galilee (Fig1) in a seismically active area as part of the Dead Sea Rift (DSR). In this area landslides and faulted and tilted blocks shape the steep, 600 m high slopes of the southern Golan Heights. The Miocene–to-Quaternary sequence which is exposed on these slopes is composed of sedimentary rocks such as marls, sand, fluvial sediments, lake sediments and basalts of Pliocene-Pleistocene age. This geological setting and lithology enhance development of compound landslides of several kinds (e.g. earth flow, slump, creep) with slide units comprising, in places, complete rock sequences. The faulting, the westward dipping strata and the steep slopes play significant roles in the sliding process, resulting in a terraced morphology of these steep slopes.

Three trenches were opened crossing three of the mapped N-S oriented normal faults composing 800 m wide fault zone (Fig 1). These faults are ~ 200 m apart from each other, crossing a series of tilted blocks .

TEG –A (Fig 2a)

A normal fault displacing the slope of one of the tilted blocks. This tilted block is composed mainly of intercalation of chalky limestone (slightly sandy) of the Maresha Formation (Middle Eocene). The fault scarp is partly covered by colluvial material towards the top and part of the scarp has a free face exposing the chalky limestone of the Maresha Formation. The paleoseismological analysis revealed that the fault is a multiple type with two identifiable faulting events. The age of the faulted slope is between 47±8 ka and 3.5±1.4. The slope which was stable during the upper Pleistocene was faulted twice during the Holocene with one event during the early Holocene (~ 11 ka) displacing ~ 1m (colluvial wedge 3) and another event during the late Holocene (~ 3.5 ka) displacing ~80 cm (colluvial wedge 4). The fresh rocky free face, which is exposed more to the north along the fault trace, might suggest that an additional faulting event occurred later than the last dated event (< 3.5±1.4 ka).

TEG - B (Fig 2b)

A normal eastern fault crossing a tilted block is displacing the Hordos and En Gev formations. The faulted slope has a minimal age of 78.6±13 ka.
Three events were identified; two that occurred close in time (during the late Pleistocene) and one that occurred during the Holocene after a long quiescence of about 35 ky. The last event, which occurred ~ 5.7±2.2 ka, displaces the slope by ~ 40 cm and was also detected in trench TEG – A, a parallel fault line located more to the west (Fig1).

TEG – C (Fig 2c)

A fault displacing the toe of the two landslides in the study site was trenched (Fig 1). The trench was opened along the southern margin of the southern landslide (Fig 1). The trenched area is composed mostly of colluvial material (unit 3) partly derived from the white-yellowish sandstone of the En-Gev formation exposed at the upper part of the slope (unit 5) and partly composed of limestone and chert lithoclasts. The colluvium is mostly rock supported with large angular rock blocks, some of which reach 50 cm, and gravel ~ 15 cm. The matrix is composed of unsorted coarse silt, sand, grit and granules. Calcic soil developed in this unit. The calcium carbonate envelopes the gravel and is disseminated in the sandy matrix. The soil reached stage II-III. At the fault zone, which is ~ 1 m wide, the colluvial unit 3 and 1 are intensely cracked and jointed (between 1–2 mm and 5-10 cm wide joints) (Fig 2).

Phase 1: Displacement of unit 3 by about 1.60 m which occurred ~ 37±3 ka (at TEG - C ~ 36 ka). The faulted unit is composed of sand (coarse and fine) with small amounts of silt and gravel of 3-4 cm size. The gravel is composed of sandstone, limestone and chert. Calcic soil developed in this unit and reached stage II-III with calcium carbonate enveloping the gravel and disseminated in the sandy matrix. The age of this unit in the downthrown block is 255±19 ka (Fig 2c; TEG-45). At the fault zone (Fig 2c; TEG-43) and in the upthrown block close to the surface (Fig 2c; TEG 46) the age of unit 3 is 97±18 and 99±12 ka, respectively. The colluvial unit 2 which is deposited on top of unit 3 on the downthrown block is composed of massive clay-silty colluvium mixed with small gravel (3-5 cm). A calcic soil developed in this unit and reached stage II-III. Most of the calcium carbonate is deposited in the upper 1 m of the unit, with decreasing amounts downward. Orthic and disorthic calcium carbonate nodules are scattered in the fine matrix, most of them ~ 2 mm. Some of the gravel is coated with calcic crust. The disorthic nodules and the coated clasts scattered in the colluvium are the result of soil erosion and deposition on the downfaulted block. The orthic calcic nodules were formed during the quiescence in between the tectonic events.

Phase 2: The second tectonic event occurred ~ 9 ka ago (Fig 2c), displacing the slope by ~40 cm. As a result, colluvial unit 1 was deposited on the downthrown block and covered the whole slope. This colluvial unit (unit 1) is composed of unsorted gravel which ranges between 20 cm, the

largest, and 3 cm, the smallest. In addition, granules of the size of 0.5 – 1 cm are also scattered in the matrix. The matrix is composed of silt and fine sand and a high amount of organic material. A weak clayey-gypsic soil developed continuously along the slope and integrated into the calcic soil at unit 2.

Two events were identified in this trench. One occurred at ~ 37 ka (Fig.2c ;TEG-42: 37±3) and another occurred ~ 9 ka ago (TEG- 44; 9.2±1.9). The well-developed soil in unit 2 and the weak soil profile in unit 1 point to a long quiescence between events.

Summary

The oldest event occurred ~ 37 ka ago and was detected in two of the trenches, TEG-B and TEG-C. Another event occurred ~ 11 ka ago and was detected in all three trenches studied. The youngest event was detected in TEG-A and occurred ~3 ka ago.
A magnitude of Mw 6.6 was estimated. The calculated magnitude ranges between Mw 6.3 and Mw 6.8 and was estimated as Mw 6.6. The recurrence time of large earthquakes on this segment is ~ 9 ky.

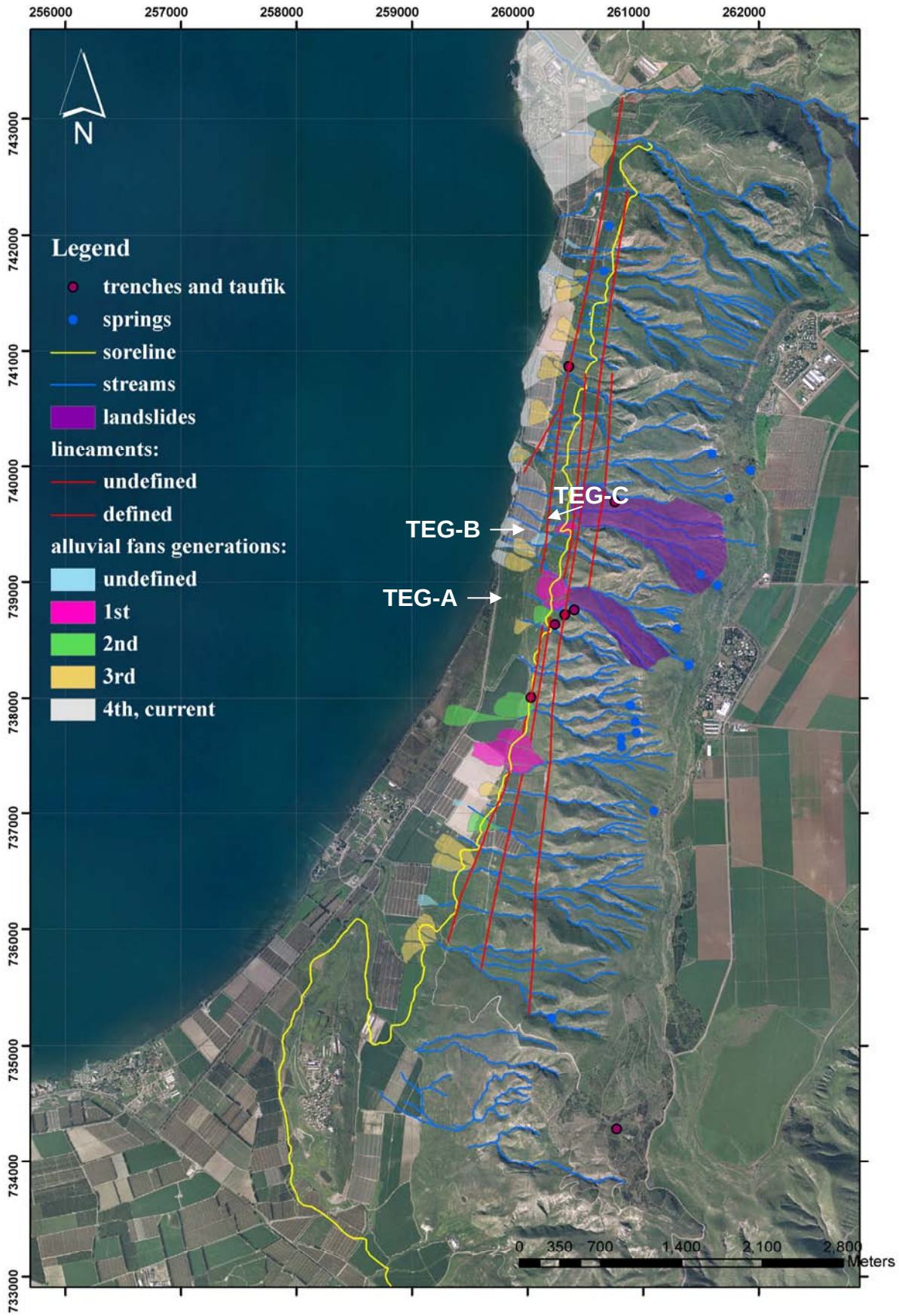

Figure 1: Morphotectonic map of the Eastern Sea of Galilee

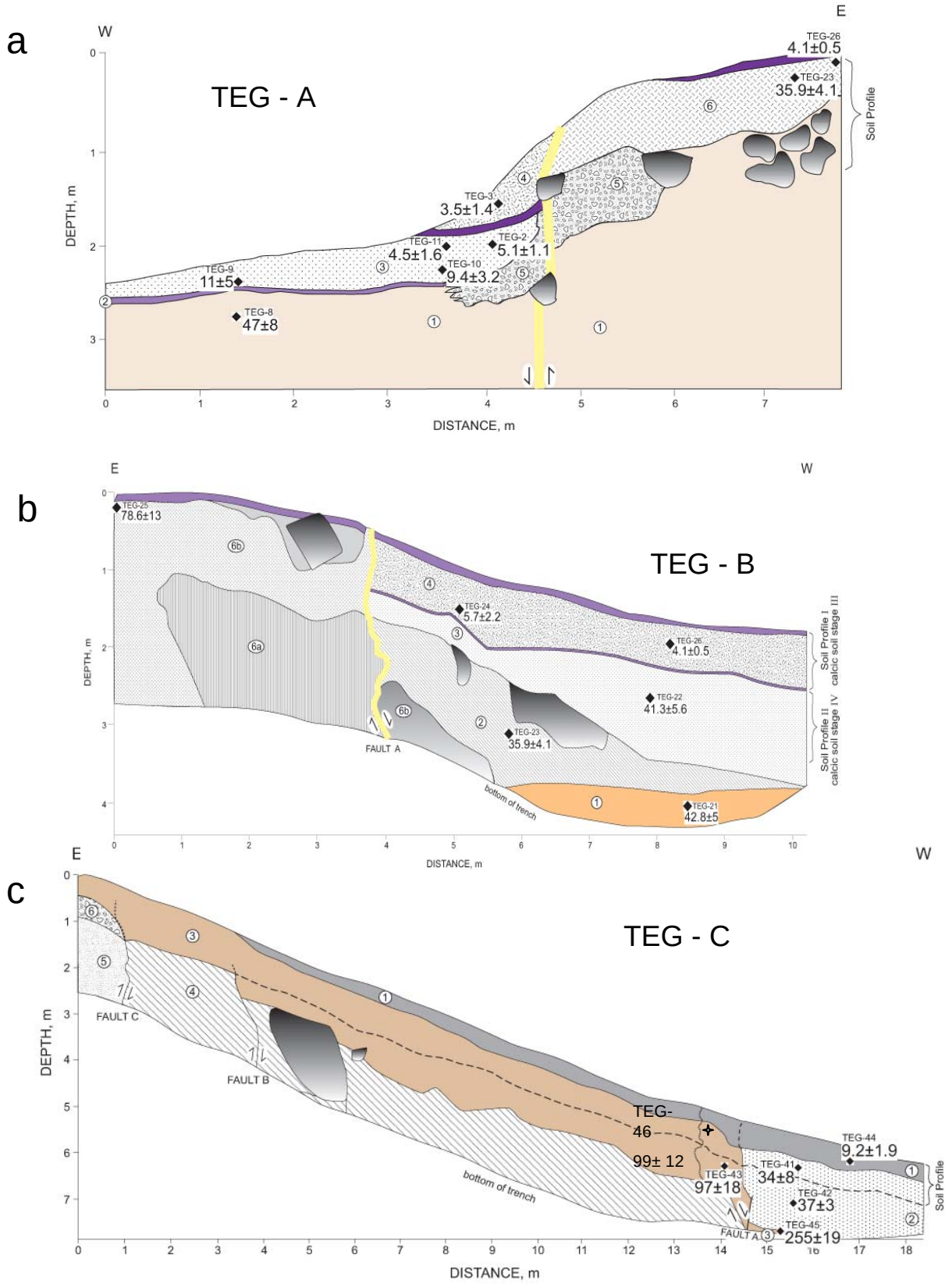

Figure 2: Paleoseismic trenches: (a) Two events: ~ 11ka and ~ 4ka; (b) two events: ~ 40ka and ~ 4 ka; (c) Two events: ~ 40ka and ~ 10ka